Journal of Elasticity
https://doi.org/10.1007/s10659-024-10088-3

RESEARCH

De-Hydration and Remodeling of Biological Materials: Swelling Theory for Multi-Domain Bodies

Michele Curatolo[1] · R.G.M. van der Sman[2] · Luciano Teresi[3]

Received: 17 May 2024 / Accepted: 6 September 2024
© The Author(s) 2024

Abstract
Biological materials always exhibit heterogeneous physical properties, both mechanical and chemical, which give them a rich phenomenology that poses significant challenges in the developing of effective models. The Flory–Rehner theory revolutionized our understanding of the dynamics of the liquid-polymers coupling in soft swollen gels, recognizing polymers as elastic networks stretched by the presence of liquid. Despite its foundational role, applying this theory to bodies with non uniform physical properties requires further improvements. This article proposes a unified approach to address mechano-diffusion challenges in multi-domain bodies, that is in material bodies made of regions having different chemo-mechanical properties, and focuses on the dehydration and remodeling of biological-like materials. Drawing inspiration from natural systems, we integrate principles from nonlinear mechanics and swelling theories; in particular, what is specifically new is the idea of applying the notion of the multiplicative decomposition of the strain–developed for plasticity–to model the swelling properties of a body made of two or more materials. The article gives a systematic presentation of the subject, and guides readers through key concepts and practical insights, aiming to provide a robust framework for modeling chemo-mechanical interactions. Moreover, it paves the way for the modeling of heterogenous bodies having spatially-varying properties.

Keywords Polymer gels · Swelling · Multi-domain polymers · Mechano-diffusion · Nonlinear mechanics

Mathematics Subject Classification 74-10 · 74-B20

✉ L. Teresi
luciano.teresi@uniroma3.it

M. Curatolo
michele.curatolo@uniroma3.it

R.G.M. van der Sman
ruud.vandersman@wur.nl

1 Dept. Architecture, Università Roma Tre, Rome, Italy

2 Wageningen-Food & Biobased Research, Wageningen University & Research, Wageningen, The Netherlands

3 Dept. Industrial Engineering, Electronic, Mechanics, Università Roma Tre, Rome, Italy

Published online: 25 September 2024

Content courtesy of Springer Nature, terms of use apply. Rights reserved.

1 Introduction

Our work centers on multi-domain, swellable bodies, characterized by diverse chemo-mechanical composition within distinct regions called domains. Biological matter, often soft and hydrated, are a prime example of this type of materials. As a result, volume change due to growing or swelling in biological tissues will behave differently in the different domains of the material. Thus, remodeling refers to the process of liquid movement and the associated non-uniform shape changes driven by chemo-mechanical inputs, and implies both a change in physical properties (as liquid concentration and apparent stiffness), and in shape. These kinds of phenomena are typical for biomaterials [7, 50, 64], and food materials [3, 8, 27, 32, 45, 48, 51, 60]; in particular, food materials can undergo considerable shrinkage during drying, or cooking — as in the case of meat, that changes both shape and texture.

Despite the ubiquity of phenomena involving large deformations coupled with water exchange, the mechanical modeling of food materials is still underdeveloped. Many fruits and vegetables have a skin much stiffer than their soft core; this asymmetry in materials properties yields specific phenomena like wrinkling [15, 40, 68]. Moreover, many food materials which are homogeneous at early stages of development, undergo material remodeling as stiffening during their maturation [20, 27, 28, 56]; as example, the case hardening in vegetables, that is the development of skin during drying [27, 35, 36]. Next to wrinkling, skin formation might also trigger the development of cavities as consequence of the drying of food droplets [5, 19, 55], or of porosity in vegetable tissue [33, 37, 57, 61, 62].

The above mentioned wrinkling and cavity formations are examples of mechanical instabilities due to the non-linearity of the stress-diffusion problem coupled with the heterogeneity of the mechanical properties. This topic of mechanical instabilities in core/shell materials is quite popular in the field of soft matter [1, 13, 26, 34, 39, 43, 44, 63, 65, 67, 71]. Such instabilities are also exploited by plants as a high-powered mechanism for seed dispersal [54], or for the morphing of plant organs [24, 52].

Only a few studies [18, 31, 69, 70] have addressed these mechanical instabilities in soft matter made of multiple domains with varying mechanical properties; in such problems, instability are driven by either swelling or dehydration - thus requiring to solve the mechano-diffusion problem. Most of these studies assume as reference configuration an initial, free-swollen state, as in [18, 69, 70], or an intermediate stress-free configuration as in [31]. Also for single-domain hydrogels there has been discussion about what is the proper reference configuration [53, 60].

Recent efforts have now focused on the 3D printing of hydrogels to create materials whose chemo-mechanical properties are tuned from soft to hard by increasing the cross-link density, using higher glass transition temperature co-monomers, or increasing the concentration of stiff particles in the polymer matrix [10, 22]. The challenges posed by the printability of 3D multi-domain biomaterials foster the development of advanced mechanical modeling capable of predicting their chemo-mechanical behaviour.

The physics of this problem is confounded by the requirement to solve the coupled equations of the balance of forces and the balance of mass solvent, also known as the mechano-diffusion problem [17].

Here, following [12], we put forth a modeling approach to tackle mechano-diffusion problems for multi-domain materials that is based on the theory of nonlinear elasticity with large distortions [46]; the same approach has been used to model self-contractile gels [4]. Mechano-diffusion coupled problems have been addressed in the seminal work by Flory and Rehner [23]; however, this corner-stone theory assumes that polymer network deformation

Content courtesy of Springer Nature, terms of use apply. Rights reserved.

is uniform and isotropic. This constraint has been lifted in more recent works, where a generalized Flory–Rehner theory to arbitrary large deformations has been presented [29, 30, 42]. Except for a few simple geometrical cases [60], the solution of the general problem requires FEA (Finite Element Analysis) as in [9, 29]. The model presented in [42] prompted the idea of tackling many different swelling problems, where the model equations have been solved with FEA [6, 11, 14].

In polymer physics it is claimed that the correct reference configuration is where the crosslinked polymer network is unstretched [38, 41, 49, 59, 66], which can be neither the initial dry state or the stress-free initial free-swollen state for natural bodies like bio/food materials. These natural biopolymer networks are synthesized/assembled in presence of solvent, and the biopolymers might be always stretched in the free-swollen state [53]. The c*-theorem of deGennes [16] states that crosslinking of polymers in (dilute) solutions always happens at the overlap concentration c* [21]. The realized elastic properties are also related to the c*-concentration, leading to a convenient scaling law for swollen biopolymer gels [59].

Hence, in this context our article explores a unified approach aimed at addressing mechano-diffusion challenges in multi-domain materials, where we explore two different possible choices modeling strategies. In spirit of the multiplicative decomposition used in plasticity [47], in growth of biological tissues [2], or in active gels [4, 12], we use this idea to translate between different configuration.

We will integrate the principles from nonlinear mechanics with large distortions [46] and the swelling theories providing a comprehensive framework for understanding chemo-mechanical interactions within multi-domain materials [58]. Basing on the hypotheses underlying the two theories, and using some key principles of continuum mechanics, we present a chemo-mechanical model which describes the effects of swelling for non homogeneous materials [25]. Moreover, the theory presented herein paves the way for the modeling of heterogenous bodies having both spatially-varying and time-varying properties. It is worth noting that the notion of distortion is used in our paper as a *physical parameter* describing the swelling properties; thus, remodeling refers to the non-uniform volume change due to differential swelling and to the associated shape changes. Actually, distortions can have the role of time evolutive variables, with their proper evolution law as in [4], and thus be capable of describing a more broad remodeling; as example, skin formation can be modeled as a time evolutive stiffening of a specific region of the body. Here, we refrain to delve into these more advanced modeling.

The article is structured to guide readers through a systematic journey of understanding and application. In Chap. 2, we introduce the concept of swelling compatibility, elucidating key and simple examples of drying and swelling in specimens crafted from different materials. Chapter 3, the pivotal section, lays the groundwork for our modeling approach by exploring key concepts such as distortion, ground state, and the selection of a base domain for our equations [58]. Chapter 4 ventures into the realm of balance equations governing the chemo-mechanical system, while Chap. 5 delves into the derivation of constitutive relations from considerations of free-energy and dissipation [25].

Furthermore, Chap. 6 offers practical insights through the presentation of two illustrative examples, shedding light on the application of our model and discussing significant findings. Both examples are representative of a typical phenomenon observed in fruits or vegetables, where a large soft core is wrapped by a stiff skin. When fresh, this edible matter is swollen with water and free of stress; upon de-hydration, the core domain loses much more water than the skin, and incompatibility arises.

Finally, Chap. 7 serves as a reflective conclusion, offering insights into the implications of our study and charting pathways for future research endeavors.

Content courtesy of Springer Nature, terms of use apply. Rights reserved.

Through this extensive exploration, our aim is to provide a robust framework for understanding and predicting the behavior of multi-domain materials undergoing swelling phenomena. By contributing to the advancement of material science and engineering, we endeavor to empower researchers and practitioners alike in navigating the intricacies of chemo-mechanical phenomena.

2 The Problem of Drying/Swelling Compatibility

Our prototypical multi-domain materials are fruits or vegetables, a very important kind of biological matter, where it is easy to recognize two different materials domains: a large soft core, wrapped by a stiff skin. When fresh, this edible matter is swollen with water and free from stress; upon de-hydration, the core domain loses much more water than the skin, yielding a noticeable volume reduction with wrinkling formation.

We begin by discussing the issues related to the modeling of drying/swelling of such two-domains materials, focusing on the question of the choice of a proper reference configuration. The amount of liquid that can be absorbed by a solid matrix depends on its chemo-mechanical properties; thus, a body made of two different materials prompts a non homogenous liquid exchange with the environment, yielding a swelling incompatibility that increases the stress in the specimen and generates unexpected shape changes [6], contrary to what happens in homogeneous (single domain) materials that swells isotropically, and exhibits a final shape which is equal to the initial one, but for a volume change. A thorough discussion about the notion of incompatibility in elasticity can be found in [46].

Nevertheless, in nature there are uncountable examples of swollen solids made of very different materials, having an almost steady and stress-free configuration, but where the stretch of the polymer network is balanced by chemical energy. Hence, contrary to common practice for synthetic polymer gels, the dry state can not be taken as a convenient reference state. Consequently, the choice of either the free-swollen state as the reference configuration, or a domain which is not a configuration, but which is endowed with all the information needed to describe the physical properties of the specimen under study. In our recent paper on pore formation in edible multi-materials we have chosen for the latter, especially because food materials appears to have a uniformly stretched state in the free-swollen state [61]. The elastic energy is defined via the current deformation of the material with respect to an unstretched ground state.

Figure 1 shows from left to right four plots: three configurations of a specimen whose top half (blue) is 50 times stiffer than the bottom half (red), plus the domain used to implement the model. At preparation state (A) the specimen is a cube in free-swelling conditions (zero stress); upon drying (B), the specimen attempts to expel all its liquid content but this is hampered by the fact that the soft part contains much more liquid than the stiff one, yielding a mismatch in the sought volume reduction. Eventually, the final steady state (C) does not have cubic shape and contains stress. Panel (D) shows the domain used for the modeling: it is not a configuration, that is the specimen can never achieve such a shape. The content of Fig. 1 has been produced with the model herein presented in Sect. 7.1.

We tackle the problem of drying/swelling compatibility with a simple, yet non trivial example, whilst introducing some key notions and notation. We consider two solid matrices made with material $i = 1, 2$, and having volume V_{si}. Each solid can absorb liquid until a new steady and stress-free configuration is attained, called *free-swollen state*. According to the key assumption that the solid volume V_{si} cannot change due to its incompressibility, the

Content courtesy of Springer Nature, terms of use apply. Rights reserved.

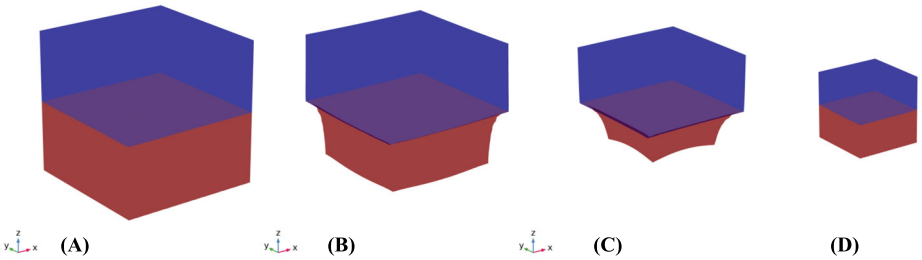

Fig. 1 (A) Preparation state of a cubic specimen whose top half (blue) is 50 times stiffer than its bottom half (red); the specimen is in a free-swelling (zero stress), steady state; (B) Change of the environment conditions triggers drying: the specimen attempts to expel all its liquid content but this is hampered by the fact that the soft part contains much more liquid than the stiff one, yielding a mismatch in the sought volume reduction. (C) The final steady state does not have cubic shape and contains stress. (D) The domain used for the modeling is not a configuration, that is the specimen can never achieve such a shape

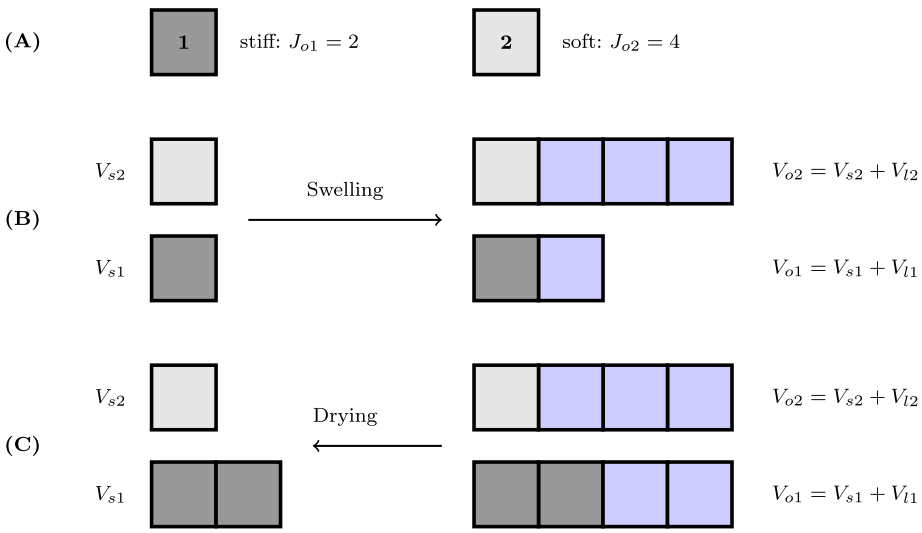

Fig. 2 Example of swelling incompatibility; each square represents a unit volume, and the amount of liquid volume is shown in cyan. (A) Two dry specimen made of a stiff (dark gray) and a soft (light gray) solid matrix, respectively, having $J_{o1} = 2$ and $J_{o2} = 4$. (B) Swelling: Two same dry volumes $V_{s1} = V_{s2}$ have different free-swollen configurations $V_{o1} \neq V_{o2}$; by glueing V_{s1} to V_{s2}, it would not be possible to have a free-swollen configuration. (C) Drying: Two same free-swollen volumes $V_{o1} = V_{o2}$ have different dry configurations $V_{s1} \neq V_{s2}$; by glueing V_{o1} to V_{o2}, it would not be possible to have a stress-free, dry configuration

free swollen volume V_{oi} is given by the sum of the solid (polymer) volume plus the volume of the liquid absorbed V_{li}, that is $V_{oi} = V_{si} + V_{li}$. The key quantities are:

$$\text{Swelling ratio: } J_{oi} = \frac{V_{oi}}{V_{si}}, \quad \text{Solid volume fraction: } \phi_{si} = \frac{1}{J_{oi}} = \frac{V_{si}}{V_{oi}}. \tag{2.1}$$

The problem of swelling incompatibility goes with the problem of the choice of a *reference configuration*, that is a region of the ambient space occupied by the material body. Figure 2 shows a cartoon with two typical examples: (A) V_{s1} (dark gray) and V_{s2} (light gray) are

Content courtesy of Springer Nature, terms of use apply. Rights reserved.

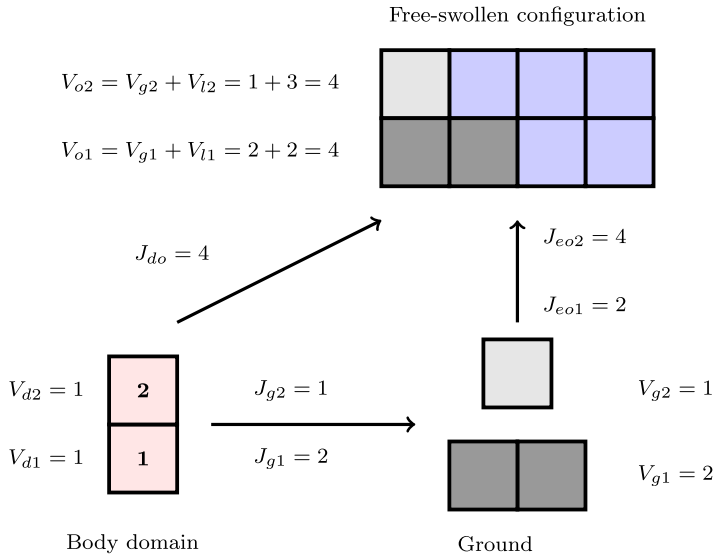

Fig. 3 The body domain $\mathcal{D} = V_{d1} \cup V_{d2}$ is the union of two subdomains having a same volumes $V_{di} = 1$. The physical properties of each subdomain are described by the maps J_{do} and J_{gi}, which give the free-swollen volume $V_{oi} = J_{do}\, V_{di}$ and the ground volume $V_{gi} = J_{gi}\, V_{di}$, respectively. The map $J_{eoi} = J_{do}\, J_{gi}^{-1}$, connecting V_{gi} to V_{oi}, is the inverse of the solid fraction. In this diagram, the only configuration is the free-swollen configuration: upon drying it will never de-swell to $\mathcal{D}$ or to $V_{g1} \cup V_{g2}$

the dry volumes of a stiff and a soft solid matrix, respectively, having different swelling features: $J_{o1} = 2$ and $J_{o2} = 4$. (B) The swelling of two same dry volumes $V_{s1} = V_{s2}$ yields two different free-swollen configurations $V_{o1} \neq V_{o2}$; by glueing together V_{s1} to V_{s2}, it would not be possible to have a free-swollen configuration. (C) The drying of two same free-swollen volumes $V_{o1} = V_{o2}$ yields two different dry configurations $V_{s1} \neq V_{s2}$; by glueing V_{o1} to V_{o2}, it would not be possible to have a stress-free, dry configuration.

The conclusion is that by choosing as reference configuration the union of V_{s1} and V_{s2} it would not be possible to describe the corresponding stress-free swollen configuration; alike it does not exist a dry configuration corresponding to a specimen made by the union of V_{o1} and V_{o2}. The problem of defining a reference configuration is quite common in continuum mechanics, and is solved by using a *body domain* instead of a configuration to define all the variables of interest: the physical properties are described by state variables defined on the body domain, which is not required to be a configuration.

To model the swelling problem described in panel (B) of Fig. 2, we consider as body domain $\mathcal{D} = V_{d1} \cup V_{d2}$, which is the union of two subdomains having same volumes V_{di}. The physical properties of each subdomain are described by: a *ground* volume $V_{gi} = J_{gi}\, V_{di}$, which represents its dry volume, and the free-swollen volume $V_{oi} = J_{do}\, V_{di}$. Thus, the whole free-swollen configuration is represented by the constant map J_{do}, whose value is given by the product of two piecewise-constant maps J_{gi} and J_{eoi}, defined on each subdomain V_{di}:

$$V_o = J_{do}\, \mathcal{D}, \quad \text{with } V_o = V_{o1} \cup V_{o2}, \quad \text{and } J_{do} = J_{eoi}\, J_{gi}. \tag{2.2}$$

The cartoon of Fig. 3 shows all the relevant quantities involved in this approach. It is worth noting that the solid fraction for each subdomain V_{di} is given by the ratio between its ground

Content courtesy of Springer Nature, terms of use apply. Rights reserved.

volume V_{gi} and its swollen one V_{oi}:

$$V_{oi} = V_{gi} + V_{li} \quad \Rightarrow \quad \text{Solid fraction: } \frac{V_{gi}}{V_{oi}} = \frac{J_{gi}}{J_{doi}} = \frac{1}{J_{eoi}}. \tag{2.3}$$

3 State Variables and Kinematics

We give a formal presentation, in the framework of continuum mechanics, of the problem depicted in the previous chapter. In particular, we augment the mechano-diffusion theory coupling it with that of nonlinear elasticity with large distortions.

Mechano-diffusion theory is based on two state variables: the first one is the *motion*, describing the current configuration of the gel; the second one is the liquid *concentration*, describing the amount of liquid content in the gel. To develop a mechano diffusion theory for multi-domain gels, we add one more state variable, the *distortion*, describing the dry and stress-free shape of volume elements. We start by discussing motion and concentration.

3.1 Motion & Liquid Concentration

Let $\mathcal{E}$ be the *Ambient Space*, that is the 3D Euclidean space; points $x \in \mathcal{E}$ are called positions. We denote with $\mathcal{V}$ the associated vector space, and with $\mathbb{L}\mathtt{in} = \mathcal{V} \otimes \mathcal{V} = \mathbb{S}\mathrm{ym} \oplus \mathbb{S}\mathrm{kw}$ the space of double tensors on $\mathcal{V}$ (linear maps of $\mathcal{V}$ into itself). A general way to describe the state of the gel is through the motion f_d and the molar concentration c_d, both defined on a point-domain $\mathcal{D}$, called *body domain*:

$$f_d : \mathcal{D} \times \mathcal{T} \to \mathcal{E}, \quad x = f_d(X_d, \tau), \quad [f_d] = \mathrm{m}; \quad c_d : \mathcal{D} \times \mathcal{T} \to \mathbb{R}, \quad [c_d] = \frac{\mathrm{mol}}{\mathrm{m}^3}. \tag{3.4}$$

Points $X_d \in \mathcal{D}$ are called body-points, or simply points; volume and area elements are dV_d and dA_d. The concentration c_d is measured per unit of body-domain volume dV_d. An alternative approach is to describe the state of the gel with respect to a *free-swollen configuration* $\mathcal{B}_o$, chosen as *reference configuration*, which is swollen with a liquid, has a spherical stress balanced by the atmospheric pressure p_{atm}, and is steady. In such a case, we use the motion f and the molar concentration c, both defined on $\mathcal{B}_o$:

$$f : \mathcal{B}_o \times \mathcal{T} \to \mathcal{E}, \quad x = f(X, \tau), \quad [f] = \mathrm{m}; \quad c : \mathcal{B}_o \times \mathcal{T} \to \mathbb{R}, \quad [c] = \frac{\mathrm{mol}}{\mathrm{m}^3}. \tag{3.5}$$

Points $X \in \mathcal{B}_o$ are called material points; volume and area elements are dV and dA. The concentration c is measured per unit of free-swollen volume dV. It is worth noting that $\mathcal{B}_o$ is usually the configuration at the *preparation state*; conversely, in general $\mathcal{D}$ is not a configuration. Given f_d and f, we define f_{do} as the map that describes $\mathcal{B}_o$ as function of $\mathcal{D}$

$$f_{do} : \mathcal{D} \to \mathcal{B}_o, \quad \text{such that } \mathcal{B}_o = f_{do}(\mathcal{D}). \tag{3.6}$$

The *current configuration* of the gel at time τ is denoted by $\mathcal{B}_\tau$. Points $x \in \mathcal{D}_t \subset \mathcal{E}$ are called *position points*, or simply, positions; volume and area elements are dv and da. The position $x \in \mathcal{D}_t$ can be described by using the motion f_d defined on $\mathcal{D}$, or by the motion f defined on $\mathcal{B}_o$; thus, we might write:

$$x = f_d(X_d, t) = X_d + \mathbf{u}_d(X_d, \tau) = f(X, t) = X + \mathbf{u}(X, \tau), \tag{3.7}$$

Content courtesy of Springer Nature, terms of use apply. Rights reserved.

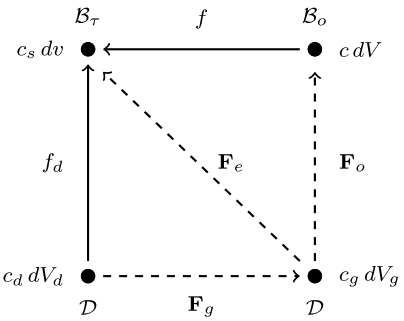

Fig. 4 The current configuration $\mathcal{B}_\tau$ can be described by using the state variables f_d, c_d defined on the body-domain $\mathcal{D}$, or by f, c defined on the free swollen configuration $\mathcal{B}_o$. The information about the zero energy state is given by three maps: the ground distortion $\mathbf{F}_g$, the free-swollen deformation $\mathbf{F}_o$, and the elastic deformation $\mathbf{F}_e = \nabla f_d\, \mathbf{F}_g^{-1} = \nabla f\, \mathbf{F}_o$. The elementary liquid content might be gauged by: $c_d\, dV_d = c_g\, dV_g = c\, dV = c_s\, dv$

where $\mathbf{u}_d$ and $\mathbf{u}$ are the displacements from $\mathcal{D}$ and $\mathcal{B}_o$, respectively. The molar liquid-content might be measured by the spatial concentration c_s per unit of current volume dv. Thus, the elementary liquid content can be gauged in different alternative ways:

$$\text{Elementary content of liquid moles} = c_d\, dV_d = c\, dV = c_s\, dv = c_g\, dV_g\,, \tag{3.8}$$

where dV_g is the volume element associated with the ground distortion $\mathbf{F}_g$ to be introduced in next Sect. 3.2. The current configuration $\mathcal{B}_\tau$ is given by:

$$\mathcal{B}_\tau = f_d(\mathcal{D}, t) = f(\mathcal{B}_o, t)\,. \tag{3.9}$$

Figure 4 shows the relations between the domain $\mathcal{D}$, and the two configurations $\mathcal{B}_o$, $\mathcal{B}_t$; the ground state can described by $\mathbf{F}_g$, defined on $\mathcal{D}$, or by $\mathbf{F}_o^{-1}$ defined on $\mathcal{B}_o$.[1] The configuration at $\tau = 0$ is denoted by $\mathcal{B}_{ini}$, and called initial configuration. Usually the initial configuration is a free swollen configuration, thus:

$$\mathcal{B}_{ini} \equiv \mathcal{B}_o = f_d(\mathcal{D}, 0) = f(\mathcal{B}_o, 0)\,, \quad \text{and} \quad f_{do}(X_d) = f_d(X_d, 0)\,. \tag{3.10}$$

Both motions f_d and f have their own key geometrical maps: the deformation gradient, or simply deformation, defined by $\mathbf{F}_d = \nabla f_d$ and $\mathbf{F} = \nabla f$; the Jacobian determinant, or simply Jacobian, $J_d = \det \mathbf{F}_d$, and $J = \det \mathbf{F}$; the co-factor or adjugate $\mathbf{F}_d^* = J_d\, \mathbf{F}_d^{-T}$, and $\mathbf{F}^* = J\, \mathbf{F}^{-T}$.

The important tangent spaces and volume elements are: the tangent space $\mathcal{T}\mathcal{D}$ to $\mathcal{D}$, called domain element, which contains both the volume elements dV_d and dV_g; the tangent space $\mathcal{T}\mathcal{B}_\tau$ to $\mathcal{B}_\tau$, called current element, with volume elements dv; the tangent space $\mathcal{T}\mathcal{B}_o$ to $\mathcal{B}_o$, with volume element dV. A cartoon of the four volume elements dV_d, dV_g, dv, dV, together with their relations is shown in Fig. 5.

We conclude by introducing two more configurations: 1) A generic *reference configuration* $\mathcal{B}_{ref} = f_{ref}(\mathcal{D})$, also called *material body*, which is an embedding of $\mathcal{D}$ in $\mathcal{E}$, chosen to

[1] Insofar, we have introduced three different domains, $\mathcal{D}$, $\mathcal{B}_o$, and $\mathcal{B}_t$, each with their own independent variables, X_d, X, and x, respectively. To avoid a cumbersome notation, with too many subscripts, we shall use a same symbol for the differential operators gradient and divergence, that is ∇ and `div`, respectively. Thus, it is the kind of function (its domain of definition) to tell between differentiation with respect to X_d, X, or x.

Content courtesy of Springer Nature, terms of use apply. Rights reserved.

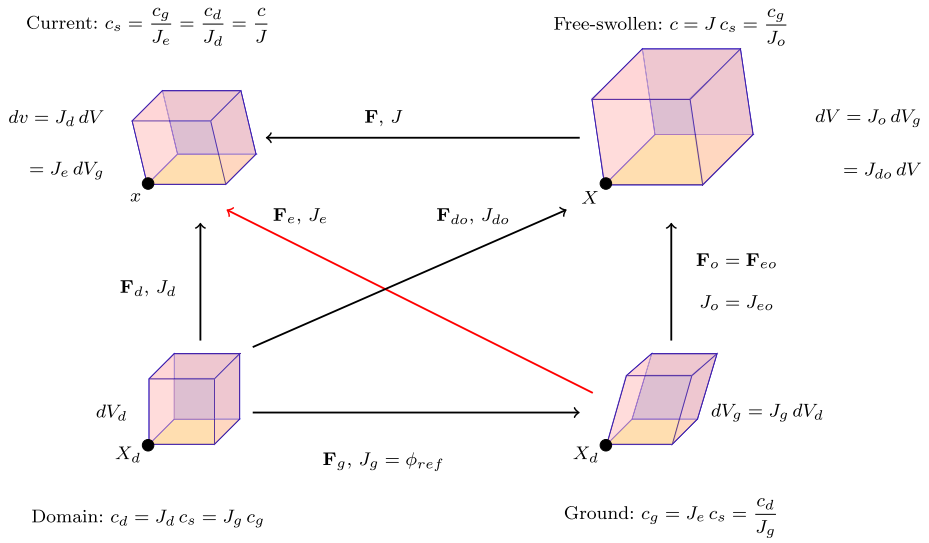

Fig. 5 Relations between the four volume elements (dV_d, dV_g, dV, dv), and the relevant deformations ($\mathbf{F}_d$, $\mathbf{F}_{do}$, $\mathbf{F}_g$, $\mathbf{F}_o$, $\mathbf{F}$, $\mathbf{F}_e$), with their determinants (J_d, J_{do}, J_g, J_o, J, J_e) connecting them. The arrow $dV_g \to dv$ is red colored, as the map $\mathbf{F}_e$ is very important: $\mathbf{C}_e = \mathbf{F}_e^T\,\mathbf{F}_e$ measures the elastic strain, while $J_e = 1/\phi_s$ is the inverse of the solid fraction ϕ_s. The maps $\mathbf{F}_{do}$, J_{do} represent the value of $\mathbf{F}_d$, J_d at the free-swollen configuration $\mathcal{B}_o$; analogously, the map $\mathbf{F}_{eo}$ connecting dV_g to dV is the value of $\mathbf{F}_e$ at $\mathcal{B}_o$, thus, $\mathbf{F}_o = \mathbf{F}_{eo}$. To get acquainted with change of frames, we also write the relation between different concentrations densities

satisfy some modeling needs; 2) The *dry configuration* $\mathcal{B}_d$, a special reference configuration containing only the solid phase, without liquid.

For many problems $\mathcal{D} \equiv \mathcal{B}_{ref}$, and f_{ref} is the identity map; nevertheless, it is of the essence to tell between a body-domain $\mathcal{D}$ and a configuration, as in many problems $\mathcal{D}$ is not a configuration.

3.2 Ground State

The *ground state* is a key notion in the theory of nonlinear elasticity with large distortions, and is a fundamental tool for many modeling problems in mechanics, as plasticity, or volumetric growth [46]. To tackle this augmented theory, the notion of volume elements is very important: a good approach is to focus on a single point and the volume element attached to it, instead of looking at a whole configuration, see Fig. 5.

The notion of ground state is a local property attributed to volume elements and it should not be confused with the notion of configuration, which has a global meaning: it is defined as the zero free-energy state of a volume element, and is described by a tensor-valued field $\mathbf{F}_g$ called distortion:

$$\mathbf{F}_g : \mathcal{D} \times \mathcal{T} \to \mathbb{L}\mathrm{in}, \quad \text{with } J_g = \det \mathbf{F}_g > 0. \tag{3.11}$$

In the present model $\mathbf{F}_g$ describes the ground state of body volume elements: in the simple example of Fig. 3, where only volume changes are considered, this role is played by $J_g = \det(\mathbf{F}_g)$; in Fig. 5, being interested in a fully 3D theory, we use $\mathbf{F}_g$ to describe also the shape of volume elements. In particular, distortions act on the domain element $\mathcal{T}\mathcal{D}$ at X_d and describe how dV_d is distorted into the volume elements dV_g whose free energy is zero.

Content courtesy of Springer Nature, terms of use apply. Rights reserved.

We note that, while the notion of deformation gradient only involves kinematics, distortions add physical information to each point of the body domain $\mathcal{D}$, as they describe the shape of a volume element which is dry and without stress. The 9 degrees of freedom associated with $\mathbf{F}_g$ might have the role of parameters, describing a given ground state, or the role of state variables, describing the time evolution of a sequence of ground states. Moreover, distortions are in general not compatible, that is, they are not the gradient of any diffeomorphism from $\mathcal{D}$, in contrast with $\mathbf{F}_d = \nabla f_d$ and $\mathbf{F} = \nabla f$ which are gradients. As a consequence, a ground configuration might not be realizable, not even locally. If such is the case, any actual configuration of $\mathcal{D}$ will be accompanied by a change of its free energy. We conclude by noting that distortions are used in our paper as a physical parameter describing the swelling properties. Actually, distortions might have the role of time evolutive variables, with their proper evolution law as in [4], and thus be capable of describing more broad remodeling processes.

3.3 Deformations & Strain Measures

Volume elements and their relations are important: the shape change of a volume element is described by a deformation tensor, and its volume change by the determinant of that tensor. We list the deformation tensors relevant for our theory, describing different shape and volume changes, whose role is shown in Fig. 5; to ease notation, we write explicitly only the point domain $\mathcal{D}$ or $\mathcal{B}_o$, and omit the time domain $\mathcal{T}$. We have:

$$
\begin{array}{llll}
\text{Domain to current} & \mathbf{F}_d = \nabla f_d : \mathcal{D} \to \mathbb{L}\mathrm{in}, & J_d = \det \mathbf{F}_d, & dv = J_d \, dV_d; \\
\text{Domain to free-swollen} & \mathbf{F}_{do} = \nabla f_{do} : \mathcal{D} \to \mathbb{L}\mathrm{in}, & J_{do} = \det \mathbf{F}_{do}, & dV = J_{do} \, dV_d; \\
\text{Free-swollen to current} & \mathbf{F} = \nabla f : \mathcal{B}_o \to \mathbb{L}\mathrm{in}, & J = \det \mathbf{F}, & dv = J \, dV. \\
\text{Domain to ground} & \mathbf{F}_g : \mathcal{D} \to \mathbb{L}\mathrm{in}, & J_g = \det \mathbf{F}_g, & dV_g = J_g \, dV_d; \\
\text{Ground to free-swollen} & \mathbf{F}_o : \mathcal{D} \to \mathbb{L}\mathrm{in}, & J_o = \det \mathbf{F}_o, & dV = J_o \, dV_g; \\
\text{Ground to current} & \mathbf{F}_e : \mathcal{D} \to \mathbb{L}\mathrm{in}, & J_e = \det \mathbf{F}_e, & dv = J_e \, dV_g;
\end{array}
\tag{3.12}
$$

It is important to tell between the domain of a deformation and its kinematical role; as example, five deformations in (3.12) are defined on $\mathcal{D}$, but their kinematical role is very different. Deformations can be composed by multiplication; as example, we have

$$
\mathbf{F}_o = \mathbf{F}_{do} \, \mathbf{F}_g^{-1}, \quad \mathbf{F} = \mathbf{F}_d \, \mathbf{F}_{do}^{-1}, \quad \mathbf{F}_d^{-1} \, \mathbf{F} \, \mathbf{F}_o \, \mathbf{F}_g = \mathbf{I}. \tag{3.13}
$$

In particular, the *elastic deformation* $\mathbf{F}_e$ might be defined as the product between $\mathbf{F}_d$ and the inverse of $\mathbf{F}_g$, or between $\mathbf{F}$ and $\mathbf{F}_o$:

$$
\mathbf{F}_e = \mathbf{F}_d \, \mathbf{F}_g^{-1} = \mathbf{F} \, \mathbf{F}_o \, . \tag{3.14}
$$

$\mathbf{F}_e$ is important from the energetic point of view as it describes the shape change between the ground volume element dV_g and the current one dv; thus, it measures the deformation between a ground volume element and it current shape. Its determinant J_e is also important from the energetic point of view as it describes the ratio between the current volume element dv and the ground one dV_g:

$$
J_e = \frac{dv}{dV_g} = \frac{J_d}{J_g} = J \, J_o. \tag{3.15}
$$

Content courtesy of Springer Nature, terms of use apply. Rights reserved.

The Jacobian J_e is the inverse of the *polymer fraction*, to be introduced later; we note that $J_o = J_{eo}$ is the ratio between the free-swollen volume element dV and the ground one dV_g. Determinants, aka Jacobians, are important for the change of volume densities; as example, the state variable c_d is a concentration per unit of material volume dV_d, while the current concentration c is a density per unit of current volume dv; they are related by $c_d = J_d\, c$; Fig. 5 shows the different concentrations that can be defined. Upon the three deformations $\mathbf{F}_d$, $\mathbf{F}_g$ and $\mathbf{F}_e$ we might define the following three different metric tensors, to be used as strain measures, known as left Cauchy-Green strains:

$$\mathbf{C}_d = \mathbf{F}_d^\top \mathbf{F}_d\,, \quad \mathbf{C}_g = \mathbf{F}_g^\top \mathbf{F}_g\,, \quad \mathbf{C}_e = \mathbf{F}_e^\top \mathbf{F}_e = \mathbf{F}_g^{-\top}\, \mathbf{C}_d\, \mathbf{F}_g^{-1}\,, \tag{3.16}$$

Analogously, we might define the following right Cauchy-Green strains:

$$\mathbf{B}_d = \mathbf{F}_d\, \mathbf{F}_d^\top\,, \quad \mathbf{B}_g = \mathbf{F}_g\, \mathbf{F}_g^\top\,, \quad \mathbf{B}_e = \mathbf{F}_e\, \mathbf{F}_e^\top = \mathbf{F}_d\, \mathbf{C}_g^{-1}\, \mathbf{F}_d^\top\,. \tag{3.17}$$

We note that $\mathbf{F}_g = \mathbf{I}$ yields $\mathbf{F}_e = \mathbf{F}_d$, and we recover the usual definitions of strain.

3.4 Volume Fractions

In polymer physics the notion of *volume fraction* is preferred to the equivalent notion of Jacobian. Each volume element dv contains both solid matter and liquid water; let dv_s and dv_w be the current solid and water volume elements: we define the following volume fractions

$$\phi_s = \frac{dv_s}{dv}, \text{ solid volume fraction;} \quad \phi_w = \frac{dv_w}{dv}, \text{ water volume fraction.} \tag{3.18}$$

The current volume element dv is the sum of the other two:

$$dv = dv_s + dv_w = (\phi_s + \phi_w)\, dv \quad \Rightarrow \quad \phi_s + \phi_w = 1\,. \tag{3.19}$$

A key hypothesis is that solid volume does not change, while water content can change due to absorption or release; thus $dv_s = dV_g$, that is the current solid volume dv_s is the same as the ground volume dV_g. It follows that the polymer fraction can be measured with $1/J_e$, or analogously with $1/(J\, J_o)$:

$$\phi_s = \frac{dv_s}{dv} = \frac{dV_g}{dv} = \frac{J_g\, dV_d}{J_d\, dV_d} = \frac{1}{J_e} = \frac{1}{J\, J_o} = \frac{1}{J}\, \frac{J_g}{J_{do}}. \tag{3.20}$$

It is worth remarking that we shall use a same symbol for the polymer fraction ϕ_s, whatever be its domain of definition; as example:

$$\phi_s = \phi_s(X_d, t) = \frac{J_g(X_d, t)}{J_d(X_d, t)}, \quad \text{or } \phi_s = \phi_s(X, t) = \frac{1}{J(X, t)\, J_o(X, t)}. \tag{3.21}$$

Usually, the physical cross-links in a network of hydro-gels are formed in presence of solvent (often water); this preparation state is a free-swollen configuration. Thus, the corresponding free-swollen polymer fraction $\phi_{so} = \phi_o$ has an important role:

$$\phi_{so} = \phi_o = \frac{dV_g}{dV} = \frac{1}{J_o} = \frac{1}{J_{eo}}. \tag{3.22}$$

Content courtesy of Springer Nature, terms of use apply. Rights reserved.

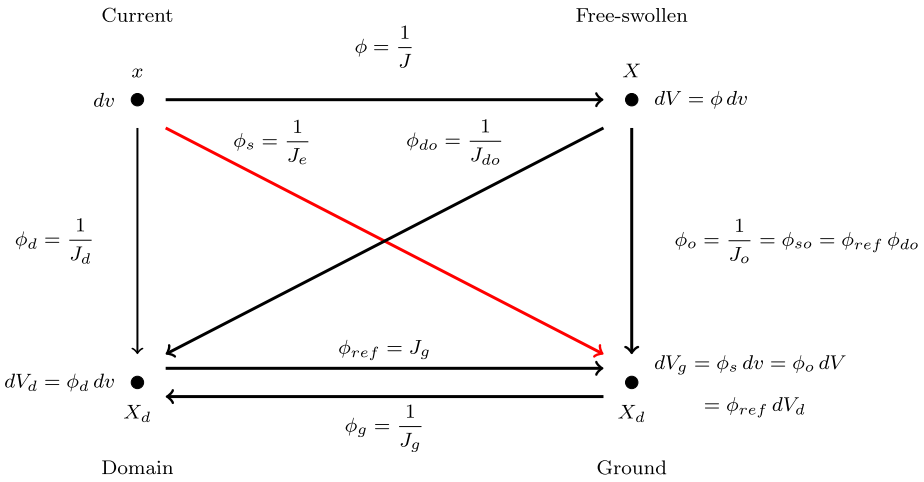

Fig. 6 Relations between the four volume elements (dV_d, dV_g, dV, dv), and the volume ratios ($\phi_d, \phi_{do}, \phi_g = 1/\phi_{ref}, \phi_o, \phi, \phi_s$) connecting them. Each volume ratio might be written as the inverse of a Jacobian. The arrow $dv \to dV_g$ is red colored, as the volume ratio ϕ_s is the polymer fraction; $\phi_o = \phi_{so}$ is the polymer fraction at the free-swollen state. Analogously, ϕ_{do} is the value of ϕ_d at X. This diagram shows also the ratio $\phi_{ref} = 1/\phi_g = J_g$

Equation $(3.19)_2$ relates water fraction to solid one; thus the water volume fraction is given by

$$\phi_w = 1 - \phi_s = \frac{dv - dv_s}{dv} = \frac{J_d - J_g}{J_d}. \tag{3.23}$$

By analogy with the relation $\phi_s = 1/J_e$, it might be convenient to define the ratios ϕ_d, ϕ_g, ϕ_o, and ϕ as follows:

$$\phi_d = \frac{dV_d}{dv} = \frac{1}{J_d},\ \phi_g = \frac{dV_d}{dV_g} = \frac{1}{J_g},\ \phi_o = \frac{dV_g}{dV} = \frac{1}{J_o},\ \phi = \frac{dV}{dv} = \frac{1}{J}. \tag{3.24}$$

We also introduce the map $\mathbf{F}_{ref} = \mathbf{F}_g^{-1}$, with $J_{ref} = \det \mathbf{F}_{ref} = 1/J_g$; then, it follows

$$J_{ref} = \frac{dV_d}{dV_g} = \frac{1}{J_g} = \phi_g, \quad \phi_{ref} = \frac{1}{J_{ref}} = \frac{dV_g}{dV_d} = J_g = \frac{1}{\phi_g}. \tag{3.25}$$

We might rewrite the diagram 5 in terms of volume fractions, see Fig. 6. We note that in Fig. 5) we show only the map $J_g = \phi_{ref}$, while in Fig. 6) we show both ϕ_g and ϕ_{ref}. We conclude this section with a list of remarks:

Remarks

- Jacobians and volume fractions are inverse to each other: the arrows connecting the four points in diagram 5 have opposite direction with respect to the arrows connecting the same four points in diagram 6.
- In diagram 5, the key map is $J_e = 1/\phi_s$ from ground dV_g to current dv;
- In diagram 6, the key map is $\phi_s = 1/J_e$ from current dv to ground dV_g.

Content courtesy of Springer Nature, terms of use apply. Rights reserved.

- Volume fractions might be composed by multiplication: the key formula relating the polymer fraction ϕ_s to ϕ_d or ϕ is (see also (3.20))

$$\phi_s = \frac{\phi_d}{\phi_g} = \phi_{ref}\,\phi_d = \phi_o\,\phi\,. \tag{3.26}$$

- From Fig. 6 we also have

$$\frac{1}{J_o} = \phi_o = \phi_{so} = \frac{\phi_{ref}}{J_{do}} \quad \Rightarrow \quad \phi_s = \phi_o\,\phi = \frac{\phi_{ref}}{J_{do}}\,\phi\,. \tag{3.27}$$

3.5 Water Content and Volumetric Constraint

From (3.8) it follows that water volume might be gauged with different molar densities. Let Ω be the molar volume of water, with $[\Omega] = \text{ mol/m}^3$; we have:

$$\text{Elementary water volume } = dv_w = \Omega\, c_d\, dV_d = \Omega\, c_g\, dV_g = \Omega\, c\, dV = \Omega\, c_s\, dv\,. \tag{3.28}$$

The previous formula yields a relation between the swelling ratios and solvent concentrations:

$$\begin{aligned} dv &= dV_g + dv_w = (J_g + \Omega\, c_d)\, dV_d = J_d\, dV_d \quad \Rightarrow \quad J_d = J_g + \Omega\, c_d\,. \\ dv &= dV_g + dv_w = \left(\frac{1}{J_o} + \Omega\, c\right) dV = J\, dV \quad \Rightarrow \quad J = \frac{1}{J_o} + \Omega\, c\,. \end{aligned} \tag{3.29}$$

Equations (3.29) yield a fundamental coupling between mechanics and chemistry: the volume changes $J_d = \det \mathbf{F}_d$ and $J = \det \mathbf{F}$, due to a displacement, must be equal to the volume changes due to water concentration:

$$\begin{aligned} J_d &= \hat{J}_d(J_g, c_d) = J_g + \Omega\, c_d = \hat{J}_d(\phi_{ref}, c_d) = \phi_{ref} + \Omega\, c_d\,; \\ J &= \hat{J}(J_o, c) = \frac{1}{J_o} + \Omega\, c = \hat{J}(\phi_o, c) = \phi_o + \Omega\, c\,. \end{aligned} \tag{3.30}$$

From the definitions of volume fractions (3.20), (3.23), and the volumetric constraint (3.30) it follows that the solid and water fraction can be represented as

$$\begin{aligned} \phi_s &= \frac{1}{J_e} = \frac{J_g}{J_d} = \frac{J_g}{J_g + \Omega\, c_d}, \qquad \text{and} \quad \phi_s = \frac{1}{J_e} = \frac{1}{J_o\, J} = \frac{1}{1 + \Omega\, J_o\, c}\,; \\ \phi_w &= 1 - \frac{1}{J_e} = \frac{J_d - J_g}{J_d} = \frac{\Omega\, c_d}{J_d}, \quad \text{and} \quad \phi_w = 1 - \frac{1}{J_o\, J} = \frac{\Omega\, J_o\, c}{1 + \Omega\, J_o\, c}\,. \end{aligned} \tag{3.31}$$

The relation between the solvent concentrations c_d and c is found by writing the elementary water content dv_{wo} of the free-swollen configuration $\mathcal{B}_o$:

$$dv_{wo} = c\, dV = c\, J_o\, dV_g = c\, J_o\, J_g\, dV_d \quad \Rightarrow \quad c_d = c\, J_o\, J_g\,. \tag{3.32}$$

When computing time rates, it is important to tell between the functions $J_d = \det \mathbf{F}_d$ and $J_d = \hat{J}_d(J_g, c_d)$; we have: $\partial/\partial t\, (\det \mathbf{F}_d) \neq \partial/\partial t\, \hat{J}_d$.

Content courtesy of Springer Nature, terms of use apply. Rights reserved.

4 Balance Equations

In the following development, only the motion and the solvent concentration will be used as state variables, while the distortion is considered as a parameter to describe the swelling properties of a given material. Balance laws can be written on the body domain $\mathcal{D}$ or on the reference configuration $\mathcal{B}_o$; nevertheless, both approaches must account for the ground state of volume elements through the distortion $\mathbf{F}_g$.

It is worth noting that the two balance laws we deal with, the Balance of Mass and the Balance of Virtual Power, are very different from each other; in particular, the second one involves mechanical power, and it originates in weak form as a duality between forces and motions.

4.1 Balance of Liquid

The balance of liquid is a mass-conservation law, and we assume that the only sources of mass are at boundary. The liquid content can be equivalently described by different molar concentrations; in the following, we shall use these three concentrations: per unit of current volume c_s, per unit of domain volume c_d, per unit of free-swollen volume c. We have:

$$\text{Liquid content} = \int_{B_\tau} \Omega\, c_s\, dv = \int_{\mathcal{D}} \Omega\, c_d\, dV_d = \int_{B_o} \Omega\, c\, dV \tag{4.33}$$

Being Ω constant, the time-rate of the liquid content involves only the concentrations c_d; thus, the balance of liquid can be stated as follows: the time-rate of liquid content, measured by moles, must be equal to the liquid source at the boundary

$$\frac{\partial}{\partial \tau}\,\text{Liquid content} = \text{Boundary source} \tag{4.34}$$

Starting from (4.34), we shall write three equivalent equations of liquid balance: i) in the current configuration $\mathcal{B}_\tau$; ii) in the body domain $\mathcal{D}$; iii) in the free-swollen configuration $\mathcal{B}_o$.

i) Liquid balance in the current configuration $\mathcal{B}_\tau$. Let $q_s = q_s(x, \tau)$ be the molar source per unit of current surface at the boundary $\partial\mathcal{B}_\tau$, with $[q_s] = \text{mol}/(\text{m}^2\ \text{s})$. The boundary source q_s can be represented in terms of the current *molar flux* $\mathbf{h}_s = \mathbf{h}_s(x, \tau)$, ($[\mathbf{h}_s] = \text{mol}/(\text{m}^2\ \text{s})$), a vector-valued quantity such that $q_s = -\mathbf{h}_s \cdot \mathbf{n}$, with $\mathbf{n}$ the normal at $\partial\mathcal{B}_\tau$; being $\mathbf{n}$ the outward normal, $-\mathbf{h}_s \cdot \mathbf{n} > 0$ implies an inward flux, and thus a positive source. From (4.33), (4.34), the definition of flux and the divergence theorem, it follows

$$\frac{\partial}{\partial \tau} \int_{\mathcal{B}_\tau} c_s\, dv = \int_{\partial\mathcal{B}_\tau} q_s\, da = -\int_{\partial\mathcal{B}_\tau} \mathbf{h}_s \cdot \mathbf{n}\, da = -\int_{\mathcal{B}_\tau} \mathtt{div}\,(\mathbf{h}_s)\, dv\,, \tag{4.35}$$

with da the surface element on $\partial\mathcal{B}_\tau$. Moreover, being $\mathcal{B}_\tau$ evolving in time, we have

$$\frac{\partial}{\partial t} \int_{\mathcal{B}_\tau} c_s\, dv = \int_{\mathcal{B}_\tau} (\dot{c}_s + \mathtt{div}\,(c_s\, \mathbf{v}))\, dv, \tag{4.36}$$

with $\mathbf{v}$ the spatial velocity defined by $\mathbf{v} \circ f_d = \dot{\mathbf{u}}_d$, or equivalently by $\mathbf{v} \circ f = \dot{\mathbf{u}}$. From standard localization arguments, (4.35), (4.36) yield the differential problem:

$$\begin{aligned}
&\dot{c}_s + \mathtt{div}\,(c_s\, \mathbf{v}) + \mathtt{div}\,(\mathbf{h}_s) = 0, && \text{bulk balance on } \mathcal{B}_\tau;\\
&q_s = -\mathbf{h}_s \cdot \mathbf{n}, && \text{boundary balance on } \partial_q\mathcal{B}_\tau;\\
&c_s = \bar{c}_s, && \text{concentration control on } \partial_c\mathcal{B}_\tau;
\end{aligned} \tag{4.37}$$

Content courtesy of Springer Nature, terms of use apply. Rights reserved.

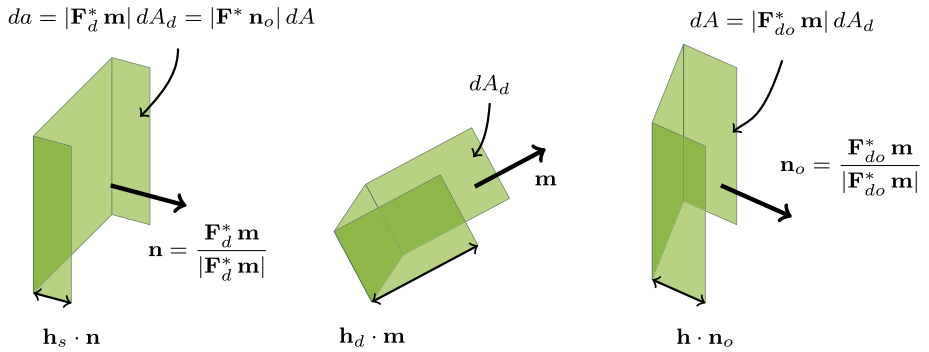

Fig. 7 Geometrical interpretation of flux. The three parallelepipeds share the same elementary volume: $\mathbf{h}_s \cdot \mathbf{n}\, da = \mathbf{h}_d \cdot \mathbf{m}\, dA = \mathbf{h} \cdot \mathbf{n}_o\, dA$; such volume measures the moles per second crossing the surfaces da (left), dA_d (center), and dA (right)

ii) Liquid balance in the body-domain $\mathcal{D}$. Balance (4.35) can be re-written on $\mathcal{D}$:

$$\frac{\partial}{\partial t} \int_{\mathcal{B}_\tau} c_s\, dv = \frac{\partial}{\partial t} \int_{\mathcal{D}} c_d\, dV_d = \int_{\mathcal{D}} \dot{c}_d\, dV_d\,, \tag{4.38}$$
$$\int_{\partial \mathcal{B}_\tau} \mathbf{h}_s \cdot \mathbf{n}\, da = \int_{\partial \mathcal{D}} \mathbf{h}_d \cdot \mathbf{m}\, dA_d = \int_{\mathcal{D}} \mathtt{div}\, \mathbf{h}_d\, dV_d\,,$$

with dA_d the surface element on $\partial\mathcal{D}$, $\mathbf{m}$ its outward normal, and $\mathbf{h}_d = \mathbf{h}_d(X_d, \tau)$ the molar flux gauged on the body-domain (the pull back of $\mathbf{h}_s$ on $\mathcal{D}$), defined by

$$\mathbf{h}_d = J_d\, \mathbf{F}_d^{-1}\, \mathbf{h}_{sd}\,, \quad \text{with } \mathbf{h}_{sd} = \mathbf{h}_s \circ f_d\,. \tag{4.39}$$

It follows that $\mathbf{h} \cdot \mathbf{n}\, da$ and $\mathbf{h}_d \cdot \mathbf{m}\, dA_d$ represent the same elementary molar rate, measured in mol/s, see Fig. 7. To the flux $\mathbf{h}_d$ it is associated a boundary source q_d per unit domain-area dA_d, given by $q_d = -\mathbf{h}_d \cdot \mathbf{m}$. From standard localization arguments, equation (4.38) yields the balance equations in differential form:

$$\begin{aligned} &\dot{c}_d + \mathtt{div}\,(\mathbf{h}_d) = 0, && \text{bulk balance on } \mathcal{D};\\ &q_d = -\mathbf{h}_d \cdot \mathbf{m}, && \text{boundary balance on } \partial_q \mathcal{D};\\ &c_d = \bar{c}_d, && \text{concentration control on } \partial_c \mathcal{D}; \end{aligned} \tag{4.40}$$

iii) Liquid balance in the free-swollen configuration $\mathcal{B}_o$; we follow the algorithm used in ii): Balance (4.35) can be re-written on $\mathcal{B}_o$:

$$\frac{\partial}{\partial t} \int_{\mathcal{B}_\tau} c_s\, dv = \frac{\partial}{\partial t} \int_{\mathcal{B}_o} c\, dV = \int_{\mathcal{B}_o} \dot{c}\, dV\,, \tag{4.41}$$
$$\int_{\partial \mathcal{B}_\tau} \mathbf{h}_s \cdot \mathbf{n}\, da = \int_{\partial \mathcal{B}_o} \mathbf{h} \cdot \mathbf{n}_o\, dA = \int_{\mathcal{B}_o} \mathtt{div}\, \mathbf{h}\, dV\,,$$

with dA the surface element on $\partial\mathcal{B}_o$, $\mathbf{m}_o$ its outward normal, and $\mathbf{h} = \mathbf{h}(X, \tau)$ the molar flux gauged on the free-swollen configuration (the pull back of $\mathbf{h}_s$ on $\mathcal{B}_o$), defined by

$$\mathbf{h} = J\, \mathbf{F}^{-1}\, \mathbf{h}_{so}\,, \quad \text{with } \mathbf{h}_{so} = \mathbf{h}_s \circ f\,. \tag{4.42}$$

Content courtesy of Springer Nature, terms of use apply. Rights reserved.

To the flux $\mathbf{h}$ is associated a boundary source q per unit domain-area dA, given by $q = -\mathbf{h}\cdot\mathbf{n}_o$. From standard localization arguments, equation (4.41) yields the balance equations in differential form:

$$\begin{aligned} &\dot{c} + \mathtt{div}\,(\mathbf{h}) = 0, && \text{bulk balance on } \mathcal{B}_o;\\ &q = -\mathbf{h}\cdot\mathbf{n}_o, && \text{boundary balance on } \partial_q\mathcal{B}_o;\\ &c = \bar{c}, && \text{concentration control on } \partial_c\mathcal{B}_o. \end{aligned} \tag{4.43}$$

We conclude by summarizing the relations between the different boundary sources (q_s, q_d, q), and fluxes $(\mathbf{h}_s, \mathbf{h}_d, \mathbf{h})$ defined insofar:

$$\begin{gathered} q_s\,da = q_d\,dA_d = q\,dA \quad\Rightarrow\quad q_d = q_s\,|\mathbf{F}_d^*\,\mathbf{m}|\,, \quad q = q_s\,|\mathbf{F}^*\,\mathbf{n}_o|\,, \quad q_d = q\,|\mathbf{F}_{do}^*\,\mathbf{m}|\,,\\ \mathbf{h}_s\cdot\mathbf{n}\,da = \mathbf{h}_d\cdot\mathbf{m}\,dA_d = \mathbf{h}\cdot\mathbf{n}_o\,dA\,,\\ \mathbf{h}_d = J_d\,\mathbf{F}_d^{-1}\,\mathbf{h}_{sd}\,, \quad \mathbf{h} = J\,\mathbf{F}^{-1}\,\mathbf{h}_{so} \quad\Leftrightarrow\quad \mathbf{h}_{sd} = \frac{1}{J_d}\,\mathbf{F}_d\,\mathbf{h}_d\,, \quad \mathbf{h}_{so} = \frac{1}{J}\,\mathbf{F}\,\mathbf{h}\,,\\ \mathbf{h}_d = J_{do}\,\mathbf{F}_{do}^{-1}\,\mathbf{h}_o \quad\Leftrightarrow\quad \mathbf{h}_o = \frac{1}{J_{do}}\,\mathbf{F}_{do}\,\mathbf{h}_d \quad \text{with } \mathbf{h}_o = \mathbf{h}\circ f_{do}. \end{gathered} \tag{4.44}$$

Remark the second subscript in the notation refers to the change of variable, see $(4.39)_2$ and $(4.42)_2$; as usually done, we shall often omit this second subscript.

4.2 Balance of Forces

The balance of forces is a conservation law for the mechanical power; it comes from the so-called *principle of virtual power* and, as for the balance of liquid, can be equivalently written on different domains. It holds:

$$\text{For any test velocity: Stress Power} = \text{Forces Power.} \tag{4.45}$$

Starting from (4.45), we shall write three equivalent balances of forces, using as test velocity the field $\tilde{\mathbf{v}}$ on $\mathcal{B}_\tau$, the field $\tilde{\mathbf{u}}_d$ on $\mathcal{D}$, and $\tilde{\mathbf{u}}$ on $\mathcal{B}_o$. The three test velocities and their gradients are related by:

$$\tilde{\mathbf{v}}\circ f_d = \tilde{\mathbf{u}}_d\,, \quad \tilde{\mathbf{v}}\circ f = \tilde{\mathbf{u}}\,, \quad \tilde{\mathbf{u}}\circ f = \tilde{\mathbf{u}}_d\,, \quad \nabla\tilde{\mathbf{v}} = \tilde{\mathbf{F}}_d\mathbf{F}_d^{-1} = \tilde{\mathbf{F}}\mathbf{F}^{-1}\,, \quad \tilde{\mathbf{F}} = \tilde{\mathbf{F}}_d\,\mathbf{F}^{-1}\,. \tag{4.46}$$

i) Principle of virtual power in the current configuration $\mathcal{B}_\tau$. Let $\mathbf{b}_s$ and $\mathbf{t}_s$ be the forces per unit of current volume and surface, respectively, and $\mathbf{T}$ the stress (Cauchy stress). Balance (4.45) writes as

$$\int_{\mathcal{B}_\tau}\mathbf{T}\cdot\nabla\tilde{\mathbf{v}}\,dv = \int_{\mathcal{B}_\tau}\mathbf{b}_s\cdot\tilde{\mathbf{v}}\,dv + \int_{\partial\mathcal{B}_\tau}\mathbf{t}_s\cdot\tilde{\mathbf{v}}\,da\,, \quad \forall\,\tilde{\mathbf{v}}\,. \tag{4.47}$$

From standard localization arguments, (4.47) yields the balance equations in differential form:

$$\begin{aligned} &\mathtt{div}\,(\mathbf{T}) + \mathbf{b} = 0, && \text{bulk balance on } \mathcal{B}_\tau;\\ &\mathbf{T}\,\mathbf{n} = \mathbf{t}, && \text{boundary balance on } \partial\mathcal{B}_\tau; \end{aligned} \tag{4.48}$$

Content courtesy of Springer Nature, terms of use apply. Rights reserved.

ii) Principle of virtual power in the body domain $\mathcal{D}$. We pull back on $\mathcal{D}$ equation (4.47); left and right hand terms yield, respectively:

$$\int_{\mathcal{B}_\tau} \mathbf{T}\cdot\nabla\tilde{\mathbf{v}}\,dv = \int_{\mathcal{D}} \mathbf{T}\cdot\tilde{\mathbf{F}}_d\,\mathbf{F}_d^{-1}\,J_d\,dV_d = \int_{\mathcal{D}} \mathbf{T}\,\mathbf{F}_d^{*}\cdot\tilde{\mathbf{F}}_d\,dV_d = \int_{\mathcal{D}} \mathbf{S}_d\cdot\tilde{\mathbf{F}}_d\,dV_d,$$
$$\int_{\mathcal{B}_\tau} \mathbf{b}_s\cdot\tilde{\mathbf{v}}\,dv + \int_{\partial\mathcal{B}_\tau} \mathbf{t}_s\cdot\tilde{\mathbf{v}}\,da = \int_{\mathcal{D}} J_d\,\mathbf{b}_s\cdot\tilde{\mathbf{u}}_d\,dV_d + \int_{\partial\mathcal{D}} |\mathbf{F}_d^{*}\,\mathbf{m}|\,\mathbf{t}_s\cdot\tilde{\mathbf{u}}_d\,dA_d\,. \tag{4.49}$$

It follows the definitions of:

$$\begin{aligned} \mathbf{S}_d &= \mathbf{T}\,\mathbf{F}_d^{*}, && \text{reference stress on } \mathcal{D};\\ \mathbf{b}_d &= J_d\,\mathbf{b}_s, && \text{force per unit of body-domain volume } dV_d;\\ \mathbf{t}_d &= |\mathbf{F}_d^{*}\,\mathbf{m}|\,\mathbf{t}_s, && \text{force per unit of body-domain surface } dA_d. \end{aligned} \tag{4.50}$$

with dA_d the surface element on $\partial\mathcal{D}$, $\mathbf{m}$ its outward normal. From standard localization arguments, (4.49) yields the balance equations in differential form:

$$\begin{aligned} &\mathtt{div}\,(\mathbf{S}_d) + \mathbf{b}_d = 0, && \text{bulk balance on } \mathcal{D};\\ &\mathbf{S}_d\,\mathbf{m} = \mathbf{t}_d, && \text{boundary balance on } \partial\mathcal{D}; \end{aligned} \tag{4.51}$$

iii) Principle of virtual power in the free swollen domain $\mathcal{B}_o$. We pull back on $\mathcal{B}_o$ equation (4.47); left and right hand terms yield, respectively:

$$\int_{\mathcal{B}_\tau} \mathbf{T}\cdot\nabla\tilde{\mathbf{v}}\,dv = \int_{\mathcal{B}_o} \mathbf{T}\cdot\tilde{\mathbf{F}}\,\mathbf{F}^{-1}\,J\,dV = \int_{\mathcal{B}_o} \mathbf{T}\,\mathbf{F}^{*}\cdot\tilde{\mathbf{F}}\,dV = \int_{\mathcal{B}_o} \mathbf{S}\cdot\tilde{\mathbf{F}}\,dV,$$
$$\int_{\mathcal{B}_\tau} \mathbf{b}_s\cdot\tilde{\mathbf{v}}\,dv + \int_{\partial\mathcal{B}_\tau} \mathbf{t}_s\cdot\tilde{\mathbf{v}}\,da = \int_{\mathcal{B}_o} J\,\mathbf{b}_s\cdot\tilde{\mathbf{u}}\,dV + \int_{\partial\mathcal{B}_o} |\mathbf{F}^{*}\,\mathbf{n}_o|\,\mathbf{t}_s\cdot\tilde{\mathbf{u}}\,dA\,. \tag{4.52}$$

It follow the definitions of:

$$\begin{aligned} \mathbf{S} &= \mathbf{T}\,\mathbf{F}_d^{*}, && \text{reference stress on } \mathcal{B}_o;\\ \mathbf{b} &= J\,\mathbf{b}_s, && \text{force per unit of free swollen volume } dV;\\ \mathbf{t} &= |\mathbf{F}^{*}\,\mathbf{n}_o|\,\mathbf{t}_s, && \text{force per unit of free swollen surface } dA. \end{aligned} \tag{4.53}$$

with da_a the surface element on $\partial\mathcal{D}_s$, $\mathbf{n}_o$ its outward normal. From standard localization arguments, (4.52) yields the balance equations in differential form:

$$\begin{aligned} &\mathtt{div}\,(\mathbf{S}) + \mathbf{b} = 0, && \text{bulk balance on } \mathcal{B}_o;\\ &\mathbf{S}\,\mathbf{n}_o = \mathbf{t}, && \text{boundary balance on } \partial\mathcal{B}_o; \end{aligned} \tag{4.54}$$

Relations between the stresses are shown in diagram 8.

5 Constitutive Equations

The model needs three constitutive laws, relating the state variables to: 1) the stress; 2) the chemical potential; 3) the liquid flux. The first two laws are derived from a free-energy den-

Content courtesy of Springer Nature, terms of use apply. Rights reserved.

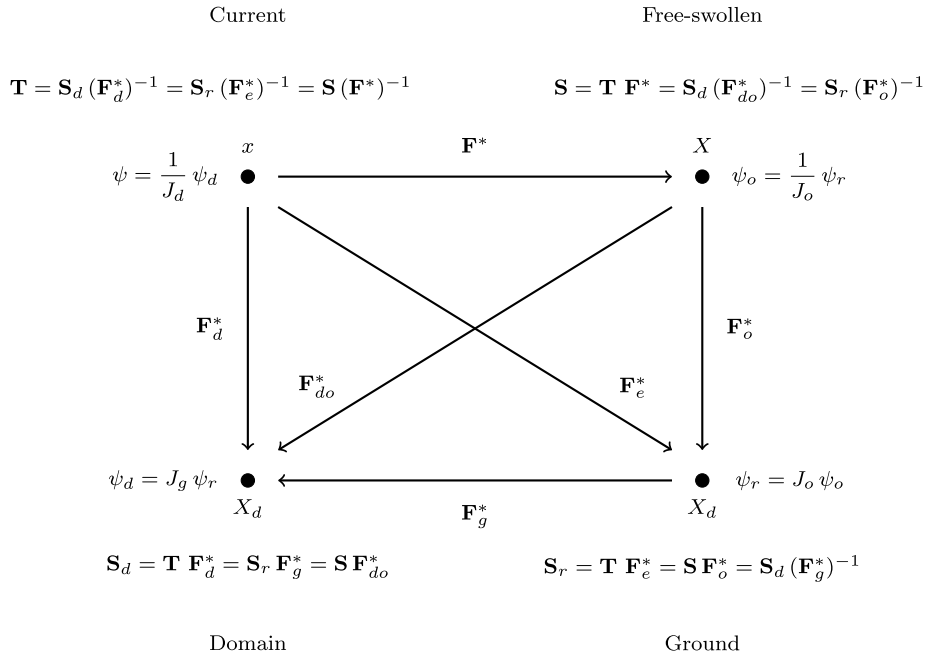

Fig. 8 Relations between the four elastic-energy densities (ψ_d, ψ_r, ψ_o, ψ), and the four stress measures ($\mathbf{S}_d$, $\mathbf{S}_r$, $\mathbf{S}$, $\mathbf{T}$). Given a deformation $\mathbf{F}_\#$, the corresponding cofactor $\mathbf{F}_\#^*$ has opposite direction

sity, which in turn might be represented with four different densities: ψ per unit of current volume; ψ_d per unit of body-domain volume, ψ_g per unit of ground volume; ψ_o per unit of free-swollen volume; these densities are related by

$$\psi\,dv = \psi_d\,dV_d = \psi_g\,dV_g = \psi_o\,dV \quad \Rightarrow \quad \begin{cases} \psi_d = J_d\,\psi = J_g\,\psi_g, \\ \\ \psi_o = \dfrac{1}{J_o}\,\psi_g = J\,\psi. \end{cases} \tag{5.55}$$

In the following, we assume ψ_g given, and we derive constitutive equations on $\mathcal{D}$ and on $\mathcal{B}_o$.

- The *free energy* ψ_g is the sum of an elastic-energy ψ_{ge} and a mixing-energy ψ_{gm}:

$$\psi_g(\mathbf{F}_e, \phi_s) = \psi_{ge}(\mathbf{F}_e) + \psi_{gm}(\phi_s). \tag{5.56}$$

- The elastic-energy $\psi_{ge} = \psi_{ge}(\mathbf{F}_e)$ only depends on the elastic deformation $\mathbf{F}_e$;
- The mixing-energy $\psi_{gm} = \psi_{gm}(\phi_s)$ only depends on the polymer fraction $\phi_s = \dfrac{1}{J_e}$;
- The *free energy* ψ_g can be pulled back $\mathcal{D}$ or pushed forward to $\mathcal{B}_o$, see (5.55):

$$\text{Pull back: } \psi_d = J_g\,\psi_g; \quad \text{Push forward: } \psi_o = \frac{1}{J_o}\,\psi_g. \tag{5.57}$$

- We define the (energetic) ground stress $\mathbf{S}_{ge}$ as:

$$\mathbf{S}_{ge} = \frac{\partial \psi_{ge}}{\partial \mathbf{F}_e}. \tag{5.58}$$

Content courtesy of Springer Nature, terms of use apply. Rights reserved.

5.1 Constitutive Equation for the Stress and the Chemical Potential

We might have many equivalent constitutive equations for the stress and the chemical potential; here we give the two representations for the stress $\mathbf{S}_d$ and the chemical potential μ_d defined on $\mathcal{D}$, and the stress $\mathbf{S}$ and the chemical potential μ defined on $\mathcal{B}_o$:

$$\begin{aligned} &\text{Domain is } \mathcal{D} \ \Rightarrow \mathbf{S}_d \text{ is dual to } \dot{\mathbf{F}}_d \text{ and } \mu_d \text{ is dual to } \dot{c}_d; \\ &\text{Domain is } \mathcal{B}_o \Rightarrow \mathbf{S} \text{ is dual to } \dot{\mathbf{F}} \text{ and } \mu \text{ is dual to } \dot{c}. \end{aligned} \tag{5.59}$$

We shall discuss the two cases in (5.59).

5.2 Constitutive Equations on a General Body Domain $\mathcal{D}$

The state variables defined on $\mathcal{D}$ are $\mathbf{u}_d$, the displacement from $\mathcal{D}$ to $\mathcal{B}_\tau$ and c_d, the molar concentration for unit of domain volume dV_d; in particular, the current position x is given by $x = X_d + \mathbf{u}_d(X_d, \tau)$. We have the following algorithm:

- Define the free energy ψ_d per unit of domain volume dV_d:

$$\psi_d = J_g\, \psi_g = J_g\, (\psi_{ge} + \psi_{gm}) = \psi_{de} + \psi_{dm}. \tag{5.60}$$

- Use the kinematical constraint (3.30), relating the displacement $\mathbf{u}_d$ to the water concentration c_d; we rewrite such a relation here:

$$J_d = \hat{J}_d(J_g, c_d) = J_g + \Omega\, c_d. \tag{5.61}$$

- Define the *relaxed free energy* Ψ_d per unit of domain volume dV_d;:

$$\Psi_d = \psi_d - p\,(J_d - \hat{J}_d), \tag{5.62}$$

  where the Lagrangian multiplier p represents a pressure.
- Compute the time rate of Ψ_d; we have

$$\begin{aligned} \dot{\Psi}_d &= \dot{\psi}_d - p\,(\dot{J}_d - \dot{\hat{J}}_d) \\ &= \frac{\partial \psi_d}{\partial \mathbf{F}_e} \cdot \dot{\mathbf{F}}_e + \frac{\partial \psi_d}{\partial \phi_s} \cdot \dot{\phi}_s - p\,(\mathbf{F}_d^* \cdot \dot{\mathbf{F}}_d - \Omega\, \dot{c}_d) \\ &= J_g\, \frac{\partial \psi_{ge}}{\partial \mathbf{F}_e} \cdot \dot{\mathbf{F}}_e + J_g\, \frac{\partial \psi_{gm}}{\partial \phi_s} \cdot \dot{\phi}_s - p\,(\mathbf{F}_d^* \cdot \dot{\mathbf{F}}_d - \Omega\, \dot{c}_d)\,. \end{aligned} \tag{5.63}$$

- Being $\mathbf{u}_d$ and c_d our state variable, we should represent $\dot{\mathbf{F}}_e$ and $\dot{\phi}_s$ in terms of $\dot{\mathbf{F}}_d$ and $\dot{c}_d$; we have

$$\begin{aligned} &\mathbf{F}_e = \mathbf{F}_d\, \mathbf{F}_g^{-1} \quad \Rightarrow \quad \dot{\mathbf{F}}_e = \dot{\mathbf{F}}_d\, \mathbf{F}_g^{-1}; \\ &\phi_s = \frac{1}{J_e} = \frac{J_g}{J_d} \quad \Rightarrow \quad \dot{\phi}_s = -\frac{J_g}{J_d^2}\, \dot{J}_d = -\frac{J_g}{J_d^2}\, \Omega\, \dot{c}_d\,. \end{aligned} \tag{5.64}$$

Content courtesy of Springer Nature, terms of use apply. Rights reserved.

- Using (5.64) and (5.58), the time rate of Ψ_d rewrites as:[2]

$$\begin{aligned}\dot{\Psi}_d &= J_g\,\mathbf{S}_{ge}\cdot\dot{\mathbf{F}}_d\,\mathbf{F}_g^{-1} - p\,\mathbf{F}_d^*\cdot\dot{\mathbf{F}}_d \\ &\quad - J_g\,\frac{\partial\psi_{gm}}{\partial\phi_s}\cdot\frac{J_g}{J_d^2}\,\Omega\,\dot{c}_d + p\,\Omega\cdot\dot{c}_d \\ &= \underbrace{\left(\mathbf{S}_{ge}\,\mathbf{F}_g^* - p\,\mathbf{F}_d^*\right)}_{\text{reference stress on }\mathcal{D}}\cdot\dot{\mathbf{F}}_d + \underbrace{\left(-\frac{\Omega}{J_e^2}\,\frac{\partial\psi_{gm}}{\partial\phi_s} + \Omega\,p\right)}_{\text{chemical potential on }\mathcal{D}}\cdot\dot{c}_d\,.\end{aligned} \tag{5.65}$$

- It follows:

$$\begin{aligned}\mathbf{S}_d &= \mathbf{S}_{ge}\,\mathbf{F}_g^* - p\,\mathbf{F}_d^*; \\ \mu_d &= -\frac{\Omega}{J_e^2}\,\frac{\partial\psi_{gm}}{\partial\phi_s} + \Omega\,p = -\Omega\,\phi_s^2\,\frac{\partial\psi_{gm}}{\partial\phi_s} + \Omega\,p; \\ \mathbf{T} &= \mathbf{S}_d\,(\mathbf{F}_d^*)^{-1} = \frac{1}{J_e}\,\mathbf{S}_{ge}\,\mathbf{F}_e^T - p\,\mathbf{I}.\end{aligned} \tag{5.66}$$

5.3 Constitutive Equations on a Free-Swollen Configuration $\mathcal{B}_o$

The state variables defined on $\mathcal{B}_o$ are $\mathbf{u}$, the displacement from $\mathcal{B}_o$ to $\mathcal{B}_\tau$ and c, the molar concentration for unit of free-swollen volume dV; in particular, the current position x is given by $x = X + \mathbf{u}(X,\tau)$. We have the following algorithm:

- Define the free energy ψ_o per unit of free-swollen volume dV:

$$\psi_o = \frac{1}{J_o}\,\psi_g = \frac{1}{J_o}\,(\psi_{ge} + \psi_{gm}) = \psi_{oe} + \psi_{om}. \tag{5.67}$$

- Use the kinematical constraint (3.30), relating the displacement $\mathbf{u}$ to the water concentration c; we rewrite such a relation here:

$$J = \hat{J}(J_o, c) = J_o^{-1} + \Omega\,c. \tag{5.68}$$

- Define the *relaxed free energy* Ψ_o per unit of free-swollen volume dV;:

$$\Psi_o = \psi_o - p\,(J - \hat{J}), \tag{5.69}$$

where the Lagrangian multiplier p represents a pressure.

[2] To highlight the duality with the time rates, we use the 'dot' notation also for the product between scalars: as example, $\mathbf{F}_d^*\cdot\dot{\mathbf{F}}_d$ is the dot product in $\mathtt{Lin}$, and $p\,\Omega\cdot\dot{c}_d$ is the product in $\mathbb{R}$.

Content courtesy of Springer Nature, terms of use apply. Rights reserved.

- Compute the time rate of Ψ_o; we have

$$\begin{aligned}\dot{\Psi}_o &= \dot{\psi}_o - p\,(\dot{J} - \dot{\hat{J}})\\ &= \frac{\partial \psi_o}{\partial \mathbf{F}_e}\cdot\dot{\mathbf{F}}_e + \frac{\partial \psi_o}{\partial \phi_s}\cdot\dot{\phi}_s - p\,(\mathbf{F}^*\cdot\dot{\mathbf{F}} - \Omega\,\dot{c}\,)\\ &= \frac{1}{J_o}\frac{\partial \psi_{ge}}{\partial \mathbf{F}_e}\cdot\dot{\mathbf{F}}_e + \frac{1}{J_o}\frac{\partial \psi_{gm}}{\partial \phi_s}\cdot\dot{\phi}_s - p\,(\mathbf{F}^*\cdot\dot{\mathbf{F}} - \Omega\,\dot{c}\,)\end{aligned} \tag{5.70}$$

- Being $\mathbf{u}$ and c our state variable, we should represent $\dot{\mathbf{F}}_e$ and $\dot{\phi}_s$ in terms of $\dot{\mathbf{F}}$ and $\dot{c}$; we have

$$\begin{aligned}&\mathbf{F}_e = \mathbf{F}\,\mathbf{F}_o \qquad\qquad \Rightarrow \quad \dot{\mathbf{F}}_e = \dot{\mathbf{F}}\,\mathbf{F}_o\\ &\phi_s = \frac{1}{J_e} = \frac{1}{J_o\,J} \quad \Rightarrow \quad \dot{\phi}_s = -\frac{\dot{J}}{J_o\,J^2} = -\frac{\Omega\,\dot{c}}{J_o\,J^2}\,.\end{aligned} \tag{5.71}$$

- Using (5.71) and (5.58), the time rate of Ψ_o rewrites as:

$$\begin{aligned}\dot{\Psi}_o &= \frac{1}{J_o}\mathbf{S}_{ge}\cdot\dot{\mathbf{F}}\,\mathbf{F}_o - p\,\mathbf{F}^*\cdot\dot{\mathbf{F}}\\ &\quad - \frac{1}{J_o}\frac{\partial \psi_{gm}}{\partial \phi_s}\cdot\frac{\Omega\,\dot{c}}{J_o\,J^2} + p\,\Omega\cdot\dot{c}\\ &= \underbrace{\left(\frac{1}{J_o}\mathbf{S}_{ge}\,\mathbf{F}_o^T - p\,\mathbf{F}^*\right)}_{\text{reference stress on } \mathcal{B}_o}\cdot\dot{\mathbf{F}}. + \underbrace{\left(-\frac{\Omega}{J_e^2}\frac{\partial \psi_{gm}}{\partial \phi_s} + \Omega\,p\right)}_{\text{chemical potential on } \mathcal{B}_o}\cdot\dot{c}.\end{aligned} \tag{5.72}$$

- It follows:

$$\begin{aligned}&\mathbf{S} = \frac{1}{J_o}\mathbf{S}_{ge}\,\mathbf{F}_o^T - p\,\mathbf{F}^*;\\ &\mu = -\frac{\Omega}{J_e^2}\frac{\partial \psi_{mr}}{\partial \phi_s} + \Omega\,p = -\Omega\,\phi_s^2\frac{\partial \psi_{mr}}{\partial \phi_s} + \Omega\,p.\\ &\mathbf{T} = \frac{1}{J}\mathbf{S}\,\mathbf{F}^T = \frac{1}{J_e}\mathbf{S}_{ge}\,\mathbf{F}_e^T - p\,\mathbf{I}.\end{aligned} \tag{5.73}$$

It is worth noting that:

- The stress is a density, thus its representation depends of the domain; conversely, the chemical potential is not a density. It follows that for $x = f_d(X_d, t) = f_o(X, t)$, we have:

$$\mathbf{S}_d(X_d, t) \neq \mathbf{S}(X, t) \neq \mathbf{T}(x, t), \quad \& \quad \mu_d(X_d, t) = \mu(X, t) = \mu_s(x, t), \tag{5.74}$$

Content courtesy of Springer Nature, terms of use apply. Rights reserved.

with μ_s the current chemical potential. Nevertheless, μ_d, μ and μ_s must be considered as distinct functions, in particular when evaluating their gradients; we have:

$$\begin{aligned} &\mu_d = \mu_s \circ f_d = \mu \circ f_{do}\,,\ \mu = \mu_s \circ f\,, \\ \Rightarrow \quad &\nabla\mu_d = \mathbf{F}_d^T\,\nabla\mu_s = \mathbf{F}_{do}^T\,\nabla\mu\,,\ \nabla\mu = \mathbf{F}^T\,\nabla\mu_s\,. \end{aligned} \tag{5.75}$$

- All the stresses turn out to be the sum of a term coming from the energy, called the elastic part, plus a reactive one due to the volumetric constraint; as example, we have:

$$\mathbf{S}_d = \mathbf{S}_{de} + \mathbf{S}_{dv}, \quad \text{with} \quad \mathbf{S}_{de} = \mathbf{S}_{ge}\,\mathbf{F}_g^*, \quad \mathbf{S}_{dv} = -p\,\mathbf{F}_d^*\,. \tag{5.76}$$

$$\mathbf{S} = \mathbf{S}_e + \mathbf{S}_v, \quad \text{with} \quad \mathbf{S}_e = \frac{1}{J_o}\,\mathbf{S}_{ge}\,\mathbf{F}_o^T, \quad \mathbf{S}_v = -p\,\mathbf{F}^*\,. \tag{5.77}$$

  We note that the reactive terms are different, $\mathbf{S}_{dv} \neq \mathbf{S}_v$, but share the same value of the pressure p. Following usual practices in mechanics, we use a same symbol for the pressure fields $p = p(X_d, t)$, $p = p(X, t)$, $p = p(x, t)$, instead of using the three names p_d, p and p_s as done for the chemical potential.
- Also μ_d, μ and μ_s turn out to be the sum of a term coming from the energy, plus another one due to the volumetric; we write only the representation for μ_d, being that for μ and μ_s similar:

$$\mu_d = \mu_{mix} + \Omega\,p, \quad \text{with} \quad \mu_{mix} = -\Omega\,\phi_s^2\,\frac{\partial\psi_{gm}}{\partial\phi_s}. \tag{5.78}$$

We conclude by checking the consistency of our stress measures:

- As expected, the current stress $\mathbf{T}$ in terms of $\mathbf{S}_{ge}$ has an unique representation, see $(5.66)_3$ and $(5.73)_3$.
- From geometry, see Fig. 8, we have

$$\begin{aligned} &\mathbf{S}_d = \mathbf{S}_r\,\mathbf{F}_g^*,\ \mathbf{S}_r = \mathbf{S}\,\mathbf{F}_o^* \Rightarrow \mathbf{S}_d = \mathbf{S}\,\mathbf{F}_o^*\,\mathbf{F}_g^*, \\ &\qquad\qquad\qquad\qquad\quad \mathbf{S} = \mathbf{S}_d\,(\mathbf{F}_g^*)^{-1}\,(\mathbf{F}_o^*)^{-1}. \\ &\mathbf{F}_e = \mathbf{F}_d\,\mathbf{F}_g^{-1} = \mathbf{F}\,\mathbf{F}_o \quad \Rightarrow \mathbf{F}_d = \mathbf{F}\,\mathbf{F}_o\,\mathbf{F}_g\,, \\ &\qquad\qquad\qquad\qquad\quad \mathbf{F}_d^* = \mathbf{F}^*\,\mathbf{F}_o^*\,\mathbf{F}_g^*,\,, \\ &\qquad\qquad\qquad\qquad\quad \mathbf{F}^* = \mathbf{F}_d^*\,(\mathbf{F}_o^*)^{-1}\,(\mathbf{F}_g^*)^{-1}. \end{aligned} \tag{5.79}$$

- From (5.79), (5.73), it follows

$$\begin{aligned} \mathbf{S}_d &= \mathbf{S}\,\mathbf{F}_o^*\,\mathbf{F}_g^* = \left(\frac{1}{J_o}\,\mathbf{S}_{ge}\,\mathbf{F}_o^T - p\,\mathbf{F}^*\right)\mathbf{F}_o^*\,\mathbf{F}_g^* \\ &= \mathbf{S}_{ge}\,\mathbf{F}_g^* - p\,\mathbf{F}_d^* = \text{equation } (5.66)_1. \end{aligned} \tag{5.80}$$

- From (5.79), (5.66), it follows

$$\begin{aligned} \mathbf{S} &= \mathbf{S}_d\,(\mathbf{F}_g^*)^{-1}\,(\mathbf{F}_o^*)^{-1} = \left(\mathbf{S}_{ge}\,\mathbf{F}_g^* - p\,\mathbf{F}_d^*\right)\,(\mathbf{F}_g^*)^{-1}\,(\mathbf{F}_o^*)^{-1} \\ &= \frac{1}{J_o}\,\mathbf{S}_{ge}\,\mathbf{F}_o^T - p\,\mathbf{F}^* = \text{equation } (5.73)_1. \end{aligned} \tag{5.81}$$

Content courtesy of Springer Nature, terms of use apply. Rights reserved.

5.3.1 Algorithm for the Stress

We summarize the steps that define the most common stress measures, whose relationships are shown in Fig. 8:

$$\begin{aligned}
\mathbf{S}_{ge} &= \frac{\partial \psi_{ge}}{\partial \mathbf{F}_e}\,, && \text{ground-energetic stress}\,;\\
\mathbf{S}_{de} &= \mathbf{S}_{ge}\,\mathbf{F}_g^*\,, && \text{pull back of the ground stress}\,;\\
\mathbf{S}_{d} &= \mathbf{S}_{de} + \mathbf{S}_{dv}\,, \quad \text{with } \mathbf{S}_{dv} = -p\,\mathbf{F}_d^*, && \text{reference stress on } \mathcal{D},\ \text{aka first P-K}\,;\\
\mathbf{S}_{e} &= \mathbf{S}_{ge}\,(\mathbf{F}_o^*)^{-1}\,, && \text{push forward of the ground stress}\,;\\
\mathbf{S} &= \mathbf{S}_{e} + \mathbf{S}_{v}\,, \quad \text{with } \mathbf{S}_{v} = -p\,\mathbf{F}^*, && \text{reference stress on } \mathcal{B}_o,\ \text{aka first P-K}\,;\\
\mathbf{T} &= \mathbf{S}_{d}\,(\mathbf{F}_d^*)^{-1} = \mathbf{S}\,(\mathbf{F}^*)^{-1}\,, && \text{current stress, aka Cauchy}\,.
\end{aligned} \tag{5.82}$$

5.3.2 Stress from Neo-Hookean Energy

The derivation of a constitutive relation for our stress measures begins with the ground elastic-energy density ψ_{ge}. We start by considering a Neo-Hookean response, that is, a strain energy density penalizing the trace (the first invariant) of the elastic strain $\mathbf{C}_e$; we set $\psi_{ge} = \psi_{NH}$:

$$\psi_{ge} = \psi_{NH}(\mathbf{C}_e) = \frac{1}{2}\,G\,(\mathbf{C}_e\cdot\mathbf{I} - 3) = \frac{1}{2}\,G\,(\mathbf{C}_d\cdot\mathbf{C}_g^{-1} - 3)\,, \quad \& \quad J_d = \hat{J}_d\,. \tag{5.83}$$

We have the following useful relations:

$$\begin{aligned}
\dot{\mathbf{C}}_e &= \dot{\mathbf{F}}_e^T\,\mathbf{F}_e + \mathbf{F}_e^T\,\dot{\mathbf{F}}_e = 2\,\mathrm{sym}\,(\mathbf{F}_e^T\,\dot{\mathbf{F}}_e)\,,\\
\dot{\psi}_{ge} &= \frac{\partial \psi_{ge}}{\partial \mathbf{C}_e}\cdot\dot{\mathbf{C}}_e = 2\,\mathbf{F}_e\,\frac{\partial \psi_{ge}}{\partial \mathbf{C}_e}\cdot\dot{\mathbf{F}}_e = \frac{\partial \psi_{ge}}{\partial \mathbf{F}_e}\cdot\dot{\mathbf{F}}_e\,,\\
\Rightarrow \quad \frac{\partial \psi_{ge}}{\partial \mathbf{F}_e} &= 2\,\mathbf{F}_e\,\frac{\partial \psi_{ge}}{\partial \mathbf{C}_e}\,.
\end{aligned} \tag{5.84}$$

Following (5.82) and (5.84), we have:

$$\begin{aligned}
&\text{Energetic stress:} && \mathbf{S}_{ge} = \frac{\partial \psi_{NH}}{\partial \mathbf{F}_e} = G\,\mathbf{F}_e = G\,\mathbf{F}_d\,\mathbf{F}_g^{-1} = G\,\mathbf{F}\,\mathbf{F}_o\,;\\
&\text{Reference stress on } \mathcal{D}: && \mathbf{S}_d = \mathbf{S}_{ge}\,\mathbf{F}_g^* - p\,\mathbf{F}_d^* = G\,J_g\,\mathbf{F}_d\,\mathbf{C}_g^{-1} - p\,\mathbf{F}_d^*\,;\\
&\text{Reference stress on } \mathcal{B}_o: && \mathbf{S} = \frac{1}{J_o}\,\mathbf{S}_{ge}\,\mathbf{F}_o^T - p\,\mathbf{F}^* = G\,\frac{1}{J_o}\,\mathbf{F}\,\mathbf{F}_o\,\mathbf{F}_o^T - p\,\mathbf{F}^*\,;\\
&\text{Current stress:} && \mathbf{T} = \mathbf{S}_d\,(\mathbf{F}_d^*)^{-1} = \mathbf{S}\,(\mathbf{F}^*)^{-1} = G\,\frac{1}{J_e}\,\mathbf{B}_e - p\,\mathbf{I}\\
& && \quad = G\,\frac{J_g}{J_d}\,\mathbf{F}_d\,\mathbf{F}_g^{-1}\,\mathbf{F}_g^{-T}\,\mathbf{F}_d^T - p\,\mathbf{I}\\
& && \quad = G\,\frac{1}{J\,J_o}\,\mathbf{F}\,\mathbf{F}_o\,\mathbf{F}_o^T\,\mathbf{F}^T - p\,\mathbf{I}\,.
\end{aligned} \tag{5.85}$$

Content courtesy of Springer Nature, terms of use apply. Rights reserved.

where $\mathbf{B}_e = \mathbf{F}_e\,\mathbf{F}_e^{\top}$. Let us note that:

- The reference stress $\mathbf{S}_e$ can be computed directly as derivative of the elastic energy density for unit of material volume dV_d

$$\mathbf{S}_{de} = \frac{\partial \psi_{de}}{\partial \mathbf{F}_d} = 2\,\mathbf{F}_d\,\frac{\partial \psi_{de}}{\partial \mathbf{C}_d} = 2\,\mathbf{F}_d\,J_g\,\frac{\partial \psi_{de}}{\partial \mathbf{C}_d} = G\,J_g\,\mathbf{F}_d\,\mathbf{C}_g^{-1} \tag{5.86}$$

- The derivative of the energy with respect to $\mathbf{E}_e = 1/2\,(\mathbf{C}_e - \mathbf{I})$ yields the second P-K stress:

$$\frac{\partial \psi_{ge}}{\partial \mathbf{E}_e} = \mathbf{F}_e^{-1}\,\mathbf{S}_{ge}\,. \tag{5.87}$$

5.3.3 Chemical Potential from Flory–Huggins Energy

The derivation of a constitutive relation for the chemical potential begins with the ground mixing-energy density ψ_{gm}. We start by considering the Flory–Huggins energy:

$$\psi_{gm}(\phi_s) = \frac{R\,T}{\Omega}\left[\left(\frac{1}{\phi_s} - 1\right)\log(1-\phi_s) + \chi\,(1-\phi_s)\right], \tag{5.88}$$

where $\chi = \chi(T)$ is the Flory parameter, possibly depending on the temperature T, and R is the universal gas constant; the ratio $R\,T/\Omega$ is a chemical energy-density, having the same physical dimensions of the shear modulus G that is $[RT/\Omega] = [G] = \mathrm{J/m^3}$. From (5.88), we have

$$\frac{\partial \psi_{gm}}{\partial \phi_s} = -\frac{R\,T}{\Omega}\,\frac{1}{\phi_s^2}\left(\log(1-\phi_s) + \chi\,\phi_s^2 + \phi_s\right), \tag{5.89}$$

and from (5.78) it follows

$$\mu_{mix} = R\,T\left(\log(1-\phi_s) + \chi\,\phi_s^2 + \phi_s\right). \tag{5.90}$$

Remarks:

- We might rewrite the chemical potential (5.90) in terms of J_e or the pair J_g and c_d as follows:

$$\begin{aligned}\mu_{mix} &= R\,T\left[\log\left(\frac{J_e - 1}{J_e}\right) + \frac{\chi}{J_e^2} + \frac{1}{J_e}\right] \\ &= R\,T\left[\log\left(\frac{\Omega\,c_d}{J_g + \Omega\,c_d}\right) + \frac{\chi\,J_g^2}{(J_g + \Omega\,c_d)^2} + \frac{J_g}{J_g + \Omega\,c_d}\right].\end{aligned} \tag{5.91}$$

- To find the chemical potential, we might also rewrite the energy (5.88) in terms of the pair J_g and c_d and then compute its time rate. We have

$$\begin{aligned}\psi_{gm} &= \frac{RT}{\Omega}\left[(J_e - 1)\,\log\left(\frac{J_e - 1}{J_e}\right) + \chi\,\frac{J_e - 1}{J_e}\right] \\ &= \frac{RT}{\Omega}\left[\frac{J_d - J_g}{J_g}\,\log\left(\frac{J_d - J_g}{J_d}\right) + \chi\,\frac{J_d - J_g}{J_d}\right].\end{aligned} \tag{5.92}$$

Content courtesy of Springer Nature, terms of use apply. Rights reserved.

Then, the time of ψ_m rate yields:

$$\dot{\psi}_m = J_g\,\dot{\psi}_{gm} = J_g\,\frac{RT}{\Omega}\left[\frac{1}{J_g}\log\left(\frac{J_d - J_g}{J_d}\right) + \frac{\chi\,J_g + J_d}{J_d^2}\right]\cdot \dot{J}_d$$

$$= RT\left[\log\left(\frac{J_d - J_g}{J_d}\right) + \frac{\chi + J_d/J_g}{(J_d/J_g)^2}\right]\cdot \dot{c}_d. \tag{5.93}$$

$$= R\,T\left[\log\left(\frac{J_e - 1}{J_e}\right) + \frac{\chi}{J_e^2} + \frac{1}{J_e}\right],$$

and we get for μ_{mix} the same formula $(5.91)_1$.

We summarize the different equivalent ways which can be used to represent the chemical potential μ_d:

$$\mu_d = \mu_d(\phi_s, p) = R\,T\left(\log(1-\phi_s) + \chi\,\phi_s^2 + \phi_s\right) + \Omega\,p\,, \quad \text{with } \phi_s = \frac{J_g}{J_d}$$

$$\mu_d = \mu_d(J_e, p) = R\,T\left[\log\left(\frac{J_e - 1}{J_e}\right) + \frac{\chi}{J_e^2} + \frac{1}{J_e}\right] + \Omega\,p\,, \quad \text{with } J_e = \frac{J_d}{J_g}$$

$$\mu_d = \mu_d(c_d, J_g, p) = R\,T\left[\log\left(\frac{\Omega\,c_d}{J_g + \Omega\,c_d}\right) + \frac{\chi\,J_g^2}{(J_g + \Omega\,c_d)^2} + \frac{J_g}{J_g + \Omega\,c_d}\right] + \Omega\,p\,. \tag{5.94}$$

We note that we are using the same notation for the three different funtcions $\mu_d = \mu_d(\phi_s, p)$, $\mu_d = \mu_d(\phi_s, p)$, and $\mu_d = \mu_d(\phi_s, p)$. An analogous representation holds for μ and μ_s; we rewrite only the analogous of $(5.94)_{1,3}$:

$$\mu = \mu(\phi_s, p) = R\,T\left(\log(1-\phi_s) + \chi\,\phi_s^2 + \phi_s\right) + \Omega\,p\,, \quad \text{with } \phi_s = \frac{1}{J}\,\frac{J_g}{J_{do}}$$

$$\mu = \mu(c, J_g, , p) = R\,T\left[\log\left(\frac{\Omega\,J_{do}\,c}{J_g + \Omega\,J_{do}\,c}\right) + \frac{\chi\,J_g^2}{(J_g + \Omega\,J_{do}\,c)^2} + \frac{J_g}{J_g + \Omega\,J_{do}\,c}\right] + \Omega\,p \tag{5.95}$$

5.4 Liquid Flux in the Bulk

In Sect. 4.1 we have introduced the liquid flux, a vector-valued surface density measuring the moles that flows through a unit surface, per unit time. Here we give the constitutive relation between the flux and the state variables, assuming the simplest one which describes the flow of a given substance from points with higher chemical potential to points with a lower one, and is consistent with the dissipation principle. We shall write three equivalent equations: i) in the current configuration $\mathcal{B}_\tau$; ii) in the body domain $\mathcal{D}$; iii) in the free-swollen configuration $\mathcal{B}_o$.

i) Constitutive relation in the current configuration $\mathcal{B}_\tau$. The molar flux $\mathbf{h}_s = \mathbf{h}_s(x, \tau)$ is given by

$$\mathbf{h}_s = -\mathbf{M}_s\,\nabla\mu_s\,. \tag{5.96}$$

Content courtesy of Springer Nature, terms of use apply. Rights reserved.

ii) Constitutive relation in the body-domain $\mathcal{D}$. The molar flux $\mathbf{h}_d = \mathbf{h}_d(X_d, t)$ is given by

$$\mathbf{h}_d = -\mathbf{M}_d \, \nabla \mu_d \, . \tag{5.97}$$

iii) Constitutive relation in the free-swollen configuration $\mathcal{B}_o$. The molar flux $\mathbf{h} = \mathbf{h}(X, \tau)$ is given by

$$\mathbf{h} = -\mathbf{M} \, \nabla \mu \, . \tag{5.98}$$

The mobilities $\mathbf{M}_\#$ are in $\mathbb{S}\mathrm{ym}^+$, the symmetric, positive-definite linear maps of $\mathbb{L}\mathtt{in}$, with $[\mathbf{M}_\#] = \ \mathrm{mol}^2/(\mathrm{s\ m\ J})$; as example $\mathbf{M}_s : \mathcal{B}_t \times \mathcal{T} \to \mathbb{S}\mathrm{ym}^+$. From (4.44) and (5.75), it follows that the three mobilities just introduced are related each other; for $\mathbf{M}_d$ and $\mathbf{M}_s$ we might write:

$$\begin{aligned} &\mathbf{h}_d = J_d \, \mathbf{F}_d^{-1} \, \mathbf{h}_{sd} = -J_d \, \mathbf{F}_d^{-1} \, (\mathbf{M}_s \, \nabla \mu_s)_d = -J_d \, \mathbf{F}_d^{-1} \, \mathbf{M}_{sd} \, \mathbf{F}_d^{-\top} \, \nabla \mu_d \, , \\ &\Rightarrow \mathbf{M}_d = J_d \, \mathbf{F}_d^{-1} \, \mathbf{M}_{sd} \, \mathbf{F}_d^{-\top} \quad \text{with } \mathbf{M}_{sd} = \mathbf{M}_s \circ f_d \, . \end{aligned} \tag{5.99}$$

For $\mathbf{M}$ and $\mathbf{M}_s$ we might write:

$$\begin{aligned} &\mathbf{h} = J \, \mathbf{F}^{-1} \, \mathbf{h}_{so} = -J \, \mathbf{F}^{-1} \, (\mathbf{M}_s \, \nabla \mu_s)_o = -J \, \mathbf{F}^{-1} \, \mathbf{M}_{so} \, \mathbf{F}^{-\top} \, \nabla \mu \, , \\ &\Rightarrow \mathbf{M} = J \, \mathbf{F}^{-1} \, \mathbf{M}_{so} \, \mathbf{F}^{-\top} \quad \text{with } \mathbf{M}_{so} = \mathbf{M}_s \circ f \, . \end{aligned} \tag{5.100}$$

For $\mathbf{M}_d$ and $\mathbf{M}$ we might write:

$$\begin{aligned} &\mathbf{h}_d = J_{do} \, \mathbf{F}_{do}{}^{-1} \, \mathbf{h}_o = J_{do} \, \mathbf{F}_{do}{}^{-1} \, (\mathbf{M} \, \nabla \mu)_o = J_{do} \, \mathbf{F}_{do}{}^{-1} \, \mathbf{M}_o \, \mathbf{F}_{do}{}^{-\top} \, \nabla \mu \, , \\ &\Rightarrow \mathbf{M}_d = J_{do} \, \mathbf{F}_{do}{}^{-1} \, \mathbf{M}_o \, \mathbf{F}_{do}{}^{-\top} \, , \quad \text{with } \mathbf{M}_o = \mathbf{M} \circ f_{do} \, . \end{aligned} \tag{5.101}$$

Any further characterization of the constitutive relation for the flux is done by specifying a law for one of the mobilities $\mathbf{M}_\# \in \mathbb{S}\mathrm{ym}^+$; here, we set

$$\mathbf{M}_d = D \, \frac{c_d}{R \, T} \, \mathbf{C}_d{}^{-1} \, , \quad \text{with } D \text{ a diffusion parameter, } [D] = \frac{\mathrm{m}^2}{\mathrm{s}} \, . \tag{5.102}$$

From (5.99), being $\mathbf{C}_d{}^{-1} = \mathbf{F}_d^{-1} \, \mathbf{F}_d^{-\top}$ and $c_d = J_d \, c_s$, it follows:

$$\mathbf{M}_{sd} = \frac{c_d}{J_d} \, \frac{D}{R \, T} \, \mathbf{I} \quad \Rightarrow \quad \mathbf{M}_s = D \, \frac{c_s}{R \, T} \, \mathbf{I} \, . \tag{5.103}$$

From (5.101), being $\mathbf{F}^{-1} = \mathbf{F}_{do} \, \mathbf{F}_d^{-1}$ and $c_d = J_{do} \, c$, it follows:

$$\mathbf{M}_o = \frac{c_d}{J_{do}} \, \frac{D}{R \, T} \, \mathbf{F}_{do} \, \mathbf{F}_d^{-1} \, (\mathbf{F}_{do} \, \mathbf{F}_d^{-1})^T \quad \Rightarrow \quad \mathbf{M} = D \, \frac{c}{R \, T} \, \mathbf{C}^{-1} \, . \tag{5.104}$$

5.5 Liquid Flux Through Interface

For the flux through an interface, we define the discrete counterpart of (5.96), that is the product $\mathbf{M}_s \, \nabla \mu_s \cdot \mathbf{n}$ becomes the scalar $m_s \, \Delta \mu_s / h_s$:

$$q_s \, da = -\mathbf{h}_s \cdot \mathbf{n} \, da = \mathbf{M}_s \, \nabla \mu_s \cdot \mathbf{n} \, da \quad \Rightarrow \quad q_s \, da = m_s \, \frac{\Delta \mu_s}{h_s} \, da \, , \tag{5.105}$$

Content courtesy of Springer Nature, terms of use apply. Rights reserved.

where $\Delta\mu_s/h_s$ represents the jump of the chemical potential over the effective thickness h_s of the interface, and $m_s = D\,c_s/(R\,T)$. Using the relations between the liquid concentrations (3.28), the gradients of the chemical potentials (5.75), and the flux sources (4.44), we might write:

$$c_s = \frac{c_d}{J_d}, \quad \Delta\mu_s = \frac{\Delta\mu_d}{J_d^{1/3}}, \quad h_s = \frac{h_d}{J_d^{1/3}}. \tag{5.106}$$

Thus, the corresponding law for q_d is given by:

$$(q_s\,da)_d = q_{sd}\,|\mathbf{F}_d^*\,\mathbf{m}|\,dA_d = \frac{D}{R\,T}\,\frac{c_d}{J_d}\,|\mathbf{F}_d^*\,\mathbf{m}|\,\frac{\Delta\mu_d}{h_d}\,dA_d = q_d\,dA_d. \tag{5.107}$$

It follows:

$$q_d = m_d\,\frac{\Delta\mu_d}{h_d}, \quad \text{with } m_d = \frac{D}{R\,T}\,\frac{c_d}{J_d}\,|\mathbf{F}_d^*\,\mathbf{m}|, \quad [m_d] = \frac{\text{mol}}{\text{m}^2\,\text{s}}\,\frac{\text{mol}}{\text{J}}. \tag{5.108}$$

Given (5.105), we follow the same algorithm to find the equivalent source density q for $\partial\mathcal{B}_o$:

$$(q_s\,da)_d = q_{so}\,|\mathbf{F}^*\,\mathbf{n}_o|\,dA = \frac{D}{R\,T}\,\frac{c}{J}\,|\mathbf{F}^*\,\mathbf{n}_o|\,\frac{\Delta\mu}{h}\;dA = q\,dA. \tag{5.109}$$

Thus, we might write:

$$q = m\,\frac{\Delta\mu}{h}, \quad \text{with } m = \frac{D}{R\,T}\,\frac{c}{J}\,|\mathbf{F}^*\,\mathbf{n}_o|, \quad [m] = \frac{\text{mol}}{\text{m}^2\,\text{s}}\,\frac{\text{mol}}{\text{J}}. \tag{5.110}$$

We note that q_d and q are related by

$$q_d = |\mathbf{F}_{do}^*\,\mathbf{m}|\,q\,, \quad q = \frac{1}{|\mathbf{F}_{do}^*\,\mathbf{m}|}\,q_d\,, \tag{5.111}$$

Equation (5.108) is used in a Neumann-like boundary condition; it yields:

$$-\mathbf{h}_d\cdot\mathbf{m} = q_d = m_d\,\frac{\Delta\mu_d}{h_d} \quad \Rightarrow \tag{5.112}$$

$$\text{water enters when } q_d > 0\,, \text{ that is when } \Delta\mu > 0\,. \tag{5.113}$$

6 Swelling of Multi-Domain Bodies

We use our mechano-diffusion model to describe swelling phenomena for bodies made of different materials, each having its own chemo-mechanical properties; for simplicity, let us consider a body made of two different materials: the body domain $\mathcal{D}$ is split into a soft domain $\mathcal{D}_s$ and a hard domain $\mathcal{D}_h$, hence $\mathcal{D} = \mathcal{D}_s \cup \mathcal{D}_h$. It follows that the boundary of each region might be split into a surface in contact with the external environment, denoted $\mathcal{S}_{ds}$ or $\mathcal{S}_{dh}$, and the interface $\mathcal{S}_{di}$ between the two regions, see Fig. 9. A hard domain $\mathcal{D}_h$ is called skin when its thickness is much smaller than the size of $\mathcal{D}$; an example of the effects of a skin is shown in Sect. 7.6. All in all, the mechano-diffusion model for multi-domain materials has three state variables: the displacement, the concentration, and the reactive pressure that enforces the volumetric constraint (3.29). The key point is that the displacement must be

Content courtesy of Springer Nature, terms of use apply. Rights reserved.

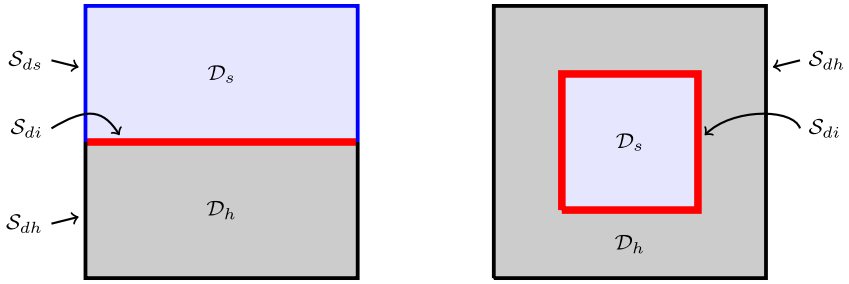

Fig. 9 Two examples of multi-domain gel. Left: $\mathcal{D}_s$ is on top of $\mathcal{D}_h$; the boundary $\partial\mathcal{D}_s$ is split into the surface $\mathcal{S}_{ds}$ in contact with the external environment, and the interface $\mathcal{S}_{di}$; the same split holds for $\partial\mathcal{D}_h$. Right: $\mathcal{D}_h$ envelopes the soft core $\mathcal{D}_s$. In this case $\partial\mathcal{D}_s = \mathcal{S}_{di}$ and $\partial\mathcal{D}_h = \mathcal{S}_{dh} \cup \mathcal{S}_{di}$. A hard domain $\mathcal{D}_h$ is called skin when its thickness is much smaller than the size of $\mathcal{D}$

continuous, while the other two state variables and the parameter describing the ground state might jump across the interface between different domains. Thus, we define on $\mathcal{D}$ a stepwise concentration c_d, pressure p, and Jacobian J_g:

$$c_d = \begin{cases} c_{\mathrm{ds}}, & \text{on } \mathcal{D}_s, \\ c_{\mathrm{dh}}, & \text{on } \mathcal{D}_h; \end{cases} \quad p = \begin{cases} p_s, & \text{on } \mathcal{D}_s, \\ p_h, & \text{on } \mathcal{D}_h. \end{cases} \quad J_g = \begin{cases} J_{\mathrm{gs}}, & \text{on } \mathcal{D}_s, \\ J_{\mathrm{gh}}, & \text{on } \mathcal{D}_h; \end{cases} \tag{6.114}$$

An analogous splitting is done for the free-swollen configuration: $\mathcal{B}_o$ is split into two bulk regions $\mathcal{B}_o = \mathcal{B}_{os} \cup \mathcal{B}_{oh}$, and we might have three possible boundaries $\mathcal{S}_{os}$, $\mathcal{S}_{oh}$ and $\mathcal{S}_{oi}$. Thus, we define a stepwise concentration c, pressure p, and Jacobian J_g:

$$c = \begin{cases} c_{\mathrm{s}}, & \text{on } \mathcal{B}_{os}, \\ c_{\mathrm{h}}, & \text{on } \mathcal{B}_{oh}; \end{cases} \quad p = \begin{cases} p_s, & \text{on } \mathcal{B}_{os}, \\ p_h, & \text{on } \mathcal{B}_{oh}. \end{cases} \quad J_g = \begin{cases} J_{\mathrm{gs}}, & \text{on } \mathcal{B}_{os}, \\ J_{\mathrm{gh}}, & \text{on } \mathcal{B}_{oh}; \end{cases} \tag{6.115}$$

It follows that for a material made of two domains, the state variables amount to seven scalar fields: 3 components of the displacement; 2 concentrations and 2 pressures. As consequence of (6.114) and (6.115), we also have jumps in J_e, J_o, and ϕ_s:

$$J_e = \begin{cases} J_{ec} = \dfrac{J_d}{J_{gc}} = \dfrac{J}{J_{oc}}, \\ \\ J_{es} = \dfrac{J_d}{J_{gs}} = \dfrac{J}{J_{os}}, \end{cases} \quad \phi_s = \begin{cases} \dfrac{1}{J_{ec}}, \\ \\ \dfrac{1}{J_{es}}. \end{cases} \tag{6.116}$$

The definition of these stepwise functions is assumed once and for all, and the specific symbols for each domain will be used in the following only when necessary. Figure 11 shows an example of the evolution of a jump in chemical potential and concentration across two domains during drying.

7 The Complete Initial, Boundary Value Problem

The model has three unknowns: two state variables, and the reactive pressure. Then, there are two balance equations, the balance of forces and of the liquid concentration, and the volumetric constraint. At first, we assume null bulk forces: $\mathbf{b}_b = \mathbf{b} = 0$.

Content courtesy of Springer Nature, terms of use apply. Rights reserved.

Then, we assume that the only chemical control is through the external chemical potential μ_{ext}; thus, we cannot control directly the concentration at the boundary, and we consider two cases:

- Concentration control: We can control the state variable c_d or c, and the pressure p through the chemical potential at the boundary μ_{ext}. Thus, the Dirichelet condition $(4.40)_3$ is replaced by the nonlinear equations:

$$\mu_d(c_d, J_g, p) = \mu_{mix}(c_d, J_g) + \Omega\, p = \mu_{ext}\,, \tag{7.117}$$

  where μ_d has been represented by $(5.94)_3$. Analogously, the Dirichelet condition $(4.43)_3$ is replaced by the nonlinear equations:

$$\mu(c, J_g, p) = \mu_{mix}(c, J_g) + \Omega\, p = \mu_{ext}\,. \tag{7.118}$$

- Flux control: To control the boundary source q_d ot q through μ_{ext} we must define a relation $\mu_{ext} \mapsto q_d$ or $\mu_{ext} \mapsto q$. Here, we shall assume (5.105), that is the current liquid source q_s is proportional to the jump $\Delta\mu_s = \mu_{ext} - \mu_s(c_s, p)$; the corresponding law for q_d and q follows from (5.108), (5.110):

$$q_d = -m_d\, \Delta\mu_d = -D\, \frac{c_d}{R\,T}\, \frac{|\mathbf{F}_d^*\, \mathbf{m}|}{J_d\, h_s}\, [\, \mu_d(c_d, J_g, p) - \mu_{ext}\,] \tag{7.119}$$

  and

$$q = -m\, \Delta\mu = -D\, \frac{c}{R\,T}\, \frac{|\mathbf{F}^*\, \mathbf{n}_o|}{J\, h_s}\, [\, \mu(c, J_g, p) - \mu_{ext}\,]\,. \tag{7.120}$$

  Thus, liquid enters when $q_d > 0$, that is $\mu_{ext} > \mu_d(c_d, J_g, p)$.

The chemical control is realized by changing μ_{ext} from $\mu_{ext} = \mu_o$ to $\mu_{ext} = \mu_\infty$; we might consider a sequence of steady problems, or a time evolutive problem:

- Sequence of n steady problems:

$$\mu_{ext} = \mu_i\,, \text{ with } i = 1, \ldots, n\,, \quad \mu_1 = \mu_o\,, \quad \mu_n = \mu_\infty\,. \tag{7.121}$$

- Time evolutive problem:

$$\mu_{ext} = \mu_{ext}(t) = \mu_o + (\mu_\infty - \mu_o)\, s(t/\tau_\mu)\,. \tag{7.122}$$

  with $s(t)$ a smooth, step-like function such that $s(0) = 0$ and $s(1) = 1$.

7.1 Initial, Boundary Value Problem on the Body Domain $\mathcal{D}$

The body domain $\mathcal{D}$ is split into two regions as described in Sect. 6. The initial, boundary value problem on $\mathcal{D} \times \mathcal{T}$ writes as follows. The balance of forces is:

$$\begin{aligned}
&0 = \mathtt{div}\, \mathbf{S}_d\,, && \text{on } \mathcal{D} \times \mathcal{T} && \text{bulk balance;}\\
&\mathbf{S}_d\, \mathbf{m} = \mathbf{t}_d\,, && \text{on } \partial_t\mathcal{D} \times \mathcal{T} && \text{control of traction;}\\
&\mathbf{u}_d = \bar{\mathbf{u}}_d\,, && \text{on } \partial_u\mathcal{D} \times \mathcal{T} && \text{control of displacement;}
\end{aligned} \tag{7.123}$$

Content courtesy of Springer Nature, terms of use apply. Rights reserved.

For the balance of liquid mass we shall always use a boundary condition as (5.108), where $\Delta\mu_d$ is the jump at the interface between two regions, or at the external boundary; the balance is split into two groups of equations. On the soft region $\mathcal{D}_s$ we have:

$$\begin{aligned}
&\dot{c}_{\mathrm{ds}} = -\mathtt{div}\,\mathbf{h}_d && \text{on } \mathcal{D}_s \times \mathcal{T} && \text{bulk balance;}\\
&q_d = -m_d\,[\,\mu_d(c_{\mathrm{ds}}, J_{\mathrm{gs}}, p_s) - \mu_{ext}\,] && \text{on } \mathcal{S}_{se} \times \mathcal{T} && \text{flux through external boundary;}\\
&q_d = -m_d\,[\,\mu_d(c_{\mathrm{ds}}, J_{\mathrm{gs}}, p_s) && \text{on } \mathcal{S}_i \times \mathcal{T} && \text{flux through interface.}\\
&\qquad - \mu_d(c_{\mathrm{dh}}, J_{\mathrm{gh}}, p_h)\,] &&&&
\end{aligned} \tag{7.124}$$

On the hard region $\mathcal{D}_h$ we have:

$$\begin{aligned}
&\dot{c}_{\mathrm{dh}} = -\mathtt{div}\,\mathbf{h}_d && \text{on } \mathcal{D}_h \times \mathcal{T} && \text{bulk balance;}\\
&q_d = -m_d\,[\,(\mu_d(c_{\mathrm{dh}}, J_{\mathrm{gh}}, p_h) - \mu_{ext}\,] && \text{on } \mathcal{S}_{he} \times \mathcal{T} && \text{flux through external boundary;}\\
&q_d = -m_d\,[\,\mu_d(c_{\mathrm{dh}}, J_{\mathrm{gh}}, p_h) && \text{on } \mathcal{S}_i \times \mathcal{T} && \text{flux through interface.}\\
&\qquad - (\mu_d(c_{\mathrm{ds}}, J_{\mathrm{gs}}, p_s)\,] &&&&
\end{aligned} \tag{7.125}$$

We note that the chemical potential is smooth in $\mathcal{D}_s$, $\mathcal{D}_h$, but it might jump at the interface $\mathcal{S}_i$, and the boundary conditions at $\mathcal{S}_i$ are the analogous of those at $\mathcal{S}_{se}$ or $\mathcal{S}_{he}$. As example, the condition $(7.125)_3$ yields:

$$\mu_d(c_{\mathrm{ds}}, J_{\mathrm{gs}}, p_s) > \mu_d(c_{\mathrm{dh}}, J_{\mathrm{gh}}, p_h) \quad \Rightarrow \quad \text{liquid flows from } \mathcal{D}_s \text{ to } \mathcal{D}_h\,. \tag{7.126}$$

Finally, we have the volumetric constraint:

$$J_d = \hat{J}_d(c_d) = J_g + \Omega\, c_d\,, \quad \text{on } \mathcal{D} \times \mathcal{T}\,. \tag{7.127}$$

7.2 Initial Conditions for $\mathcal{B}_{ini} = f_d(\mathcal{D}, 0)$

The initial configuration $\mathcal{B}_{ini}$ is not the domain $\mathcal{D}$ used for the modeling, but is chosen to be a free swollen configuration: $\mathcal{B}_{ini} = \mathcal{B}_o = f_d(\mathcal{D}, 0)$, with $\mathcal{B}_o$ corresponding to $\mu_d = 0$. Given (6.114), the initial configuration $\mathcal{B}_{ini}$ is characterized by: the initial displacement $\mathbf{u}_{do}$ in $\mathcal{D}$; the initial concentration c_{dso}, pressure p_{so} and parameter J_{gs} in $\mathcal{D}_s$; the initial concentration c_{dho}, pressure p_{ho} and parameter J_{gh} in $\mathcal{D}_h$. To set these values, we use $(5.85)_2$ for $\mathbf{S}_d$ and $(5.94)_3$ for μ_d; we assume:

$$\begin{aligned}
&\mathbf{F}_d(X_d, 0) = \mathbf{F}_{do} = \lambda_{do}\,\mathbf{I}\,, \quad \Rightarrow \mathbf{F}^*_{do} = \lambda^2_{do}\,\mathbf{I}, && \text{homogeneous deformation in } \mathcal{D};\\
&\mathbf{F}_g = \lambda_g\,\mathbf{I}, \quad \Rightarrow \mathbf{F}^*_g = \lambda^2_g\,\mathbf{I}, && \text{spherical distortion in } \mathcal{D};\\
&\mathbf{S}_d(X_d, 0) = \mathbf{S}_{ge}\,\mathbf{F}^*_g - p_o\,\mathbf{F}^*_{do} = -p_{\mathrm{atm}}\,\mathbf{F}^*_{do}, && \text{stress balanced by atmospheric pressure;}\\
&\mu_d(c_{\mathrm{dso}}, J_{\mathrm{gs}}, p_{so}) = \mu_o = 0 && \text{homogeneous chemical potential in } \mathcal{D}_s;\\
&\mu_d(c_{\mathrm{dho}}, J_{\mathrm{gh}}, p_{ho}) = \mu_o = 0 && \text{homogeneous chemical potential in } \mathcal{D}_h;
\end{aligned} \tag{7.128}$$

To determine the right values of J_{gs}, J_{gh}, $\mathbf{u}_{do}$, c_{dso}, c_{dho} and p_{so}, p_{ho} we follow this algorithm:

1. We set $J_{\mathrm{gs}} = 1$, and we tune both J_{do} and J_{gh} to get $\mu_d = 0$ in both regions.

Content courtesy of Springer Nature, terms of use apply. Rights reserved.

2. Given (7.128), the Neo-Hookean energy yields

$$\mathbf{S}_d(X_d, 0) = \mathbf{S}_{ge}\,\lambda_g^2 - p_o\,\lambda_{do}^2\,\mathbf{I} = (G\,\lambda_{do}\,\lambda_g - p_o\,\lambda_{do}^2)\,\mathbf{I} = -p_{\text{atm}}\,\lambda_{do}^2\,\mathbf{I}\,; \tag{7.129}$$

it follows that we can represent p_{os}, p_{oh} in terms of λ_{do} and λ_g:

$$p_{so} = G_s\,\frac{\lambda_{gs}}{\lambda_{do}} + p_{\text{atm}}\,, \quad p_{ho} = G_h\,\frac{\lambda_{gh}}{\lambda_{do}} + p_{\text{atm}}\,, \tag{7.130}$$

with G_s, G_h the shear moduli in $\mathcal{D}_s$ and $\mathcal{D}_h$, respectively.

3. Having assumed $J_{\text{gs}} = 1$, we start with the soft region. Using $(3.29)_1$ we can set the initial condition for c_{dso}:

$$c_{\text{dso}} = \frac{J_{do} - J_{\text{gs}}}{\Omega} = \frac{J_{do} - 1}{\Omega}. \tag{7.131}$$

4. We use $(5.94)_3$ to represent the initial chemical potential μ_o in the soft region as a function of J_{do}:

$$\begin{aligned}\mu_d(c_{\text{dso}}, J_{\text{gs}}, p_{os}) &= R\,T\,\left(\log\left(\frac{\Omega\,c_{dso}}{J_{do}}\right) + \frac{J_{gc}}{J_{do}} + \frac{\chi}{J_{do}^2}\right) + \Omega\,p_{os}\\ &= R\,T\,\left(\log\left(\frac{\Omega\,c_{dso}}{J_{do}}\right) + \frac{1}{J_{do}} + \frac{\chi}{J_{do}^2}\right) + \Omega\,\left(\frac{G_s}{J_{do}^{1/3}} + p_{\text{atm}}\right)\\ &= \mu_d(J_{\text{do}})\,.\end{aligned} \tag{7.132}$$

Solving $\mu_d(J_{\text{do}}) = 0$ yields J_{do} and $\lambda_{do} = J_{do}^{1/3}$.

5. Once J_{do} has been determined, the initial displacement is completely characterized; we have:

$$\mathbf{F}_{do} = \mathbf{I} + \nabla\mathbf{u}_d = \lambda_{do}\,\mathbf{I}, \Rightarrow \nabla\mathbf{u}_d = (\lambda_{do} - 1)\,\mathbf{I} \Rightarrow \mathbf{u}_d = (\lambda_{do} - 1)\,X_d + \text{const.} \tag{7.133}$$

As example, for a domain centered at the origin, or for a cube with side length L, centered at the corner, we have, respectively:

$$\mathbf{u}_{do} = (\lambda_{do} - 1)\,X_d\,, \quad \mathbf{u}_{do} = (\lambda_{do} - 1)\,(X_d + L/2)\,. \tag{7.134}$$

6. Then, we move to the hard region to find c_{dho}:

$$c_{\text{dho}} = \frac{J_{do} - J_{gh}}{\Omega}; \tag{7.135}$$

7. We use again $(5.94)_3$ to represent the initial chemical potential μ_o in the hard region as a function of J_{gh}:

$$\begin{aligned}\mu_d(c_{\text{dho}}, J_{\text{gh}}, p_{oh}) &= R\,T\,\left(\log\left(\frac{\Omega\,c_{dho}}{J_{do}}\right) + \frac{J_{gh}}{J_{do}} + \frac{\chi}{J_{do}^2}\right) + \Omega\,\left(\frac{G_s}{J_{do}^{1/3}} + p_{\text{atm}}\right)\\ &= \mu_d(J_{\text{gh}})\,.\end{aligned} \tag{7.136}$$

Solving $\mu_d(J_{\text{gh}}) = 0$ yields J_{gh} and $\lambda_{gh} = J_{gh}^{1/3}$.

Content courtesy of Springer Nature, terms of use apply. Rights reserved.

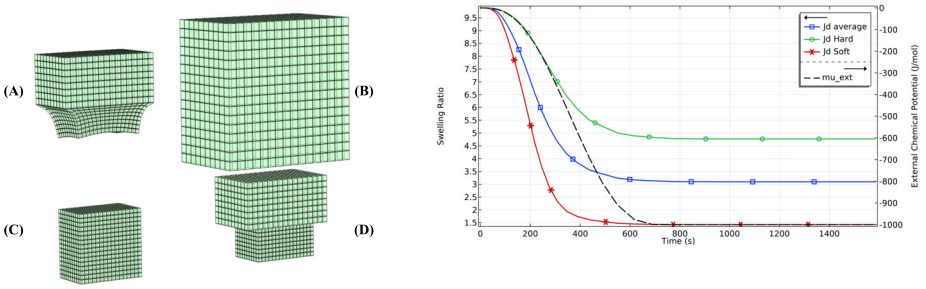

Fig. 10 Left y-axis: average swelling ratio $\bar{J}_d$ versus time, in the soft (red, star) and stiff (green, circle) part of the specimen, and for the whole specimen (blue, square). Right y-axis: external chemical potential μ_{ext} versus time (black, dashed)

Eventually, we have the right values of λ_{do}, λ_{gs} and λ_{gh} that yield a uniform configuration $\mathcal{B}_{ini} = \mathcal{B}_o$ with homogeneous chemical potential $\mu_d = \mu_o = 0$ J/mol, and homogeneous stress $\mathbf{S}_d$ satisfying the boundary conditions.

7.3 Solved Problem on $\mathcal{D}$

We solve the drying problem for a bidomain specimen cube whose top half is 50 times stiffer than the bottom half. Three configurations of the specimen are shown in Fig. 1: at preparation state $\mathcal{B}_o$, the specimen has a cubic shape and is in free-swelling conditions (A). By decreasing the external chemical potential, the configuration $\mathcal{B}_t$ of the specimen evolves in time; the expulsion of liquid content is hampered by the fact that the soft part de-swells much more than the stiff one, yielding a mismatch in the volume reduction (B). Drying stops at final state $\mathcal{B}_\infty$, and the specimen remains deformed and with stress (C). Finally, the domain $\mathcal{D}$ used for the modeling is shown in (D). Color map is blue = stiff, red = soft. It is worth noting that the specimen can never achieve such a shape.

Figure 10 (left) shows a sampling of volume elements: A) The current elements in $\mathcal{B}_\tau$ are deformed; B) All the free-swollen elements in $\mathcal{B}_o$ have a same size; C) All the domain elements in $\mathcal{D}$ have a same size as well, and are smaller than those in $\mathcal{B}_o$; D) Ground elements associated to $\mathcal{D}$ have not same size, thus describing their different swelling properties. We note that the volume elements at top are larger than that at bottom because they swell less: in this example, the ground volume elements in the soft and in the stiff regions are stretched by λ_{os} and λ_{oh}, respectively, with

$$\lambda_{os} = \frac{\lambda_{do}}{\lambda_{gs}} = \frac{2.146}{1} = 2.146\,, \quad \lambda_{oh} = \frac{\lambda_{do}}{\lambda_{gh}} = \frac{2.146}{1.428} = 1.5028. \tag{7.137}$$

Thus, the stretch from dry to free swelling conditions is $\lambda_{os} = 2.146$ for the soft polymer, and $\lambda_{oh} = 1.5028$ for the hard one. Figure 10 (right) shows the time course of the average swelling ratio J_d in the soft (red, star) and stiff (green, circle) regions of the specimen. The average swelling ratio for the whole specimen is in between (blue, square). Figure 11 shows chemical potential μ (left) and current concentration $c_s = c_d/J_d$ (right) along the current vertical coordinate $z = Z_d + w_d$ through the center of the cube, at $t = 0, 100, \ldots, 700$ s; w_d is the vertical component of the displacement $\mathbf{u}_d$. Chemical potential is smooth both at initial and final times, and has jumps during the evolution; inset (a) shows a zoom of μ at

Content courtesy of Springer Nature, terms of use apply. Rights reserved.

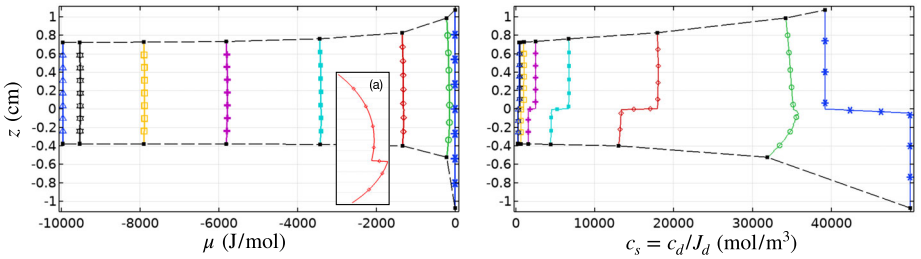

Fig. 11 Chemical potential μ (left) and current concentration $c_s = c_d/J_d$ (right) along the current vertical coordinate z through the center of the cube, at $t = 0, 100, \ldots, 700$ s. Chemical potential is smooth both at initial and final times, and has jumps during the evolution; inset (a) shows a zoom at $t = 200$ s. Concentration always jumps. Dashed black lines show the thickness evolution; time runs from right to left

Table 1 Parameters for the 3D model

L_d	=	1 [cm]	edge length of cubic domain $\mathcal{D}$
R_d	=	1 [cm]	radius and height of cylindrical domain $\mathcal{D}$
H_d	=	$R_d/50 = 0.2$ [cm]	skin thickness of cylindrical domain $\mathcal{D}$
λ_{do}	=	2.146	initial stretch $\mathcal{D} \to \mathcal{B}_o$
L_o	=	2.146 [cm]	edge length of free-swollen cube $\mathcal{B}_o$
R_o	=	2.146 [cm]	radius of free-swollen cylinder $\mathcal{B}_o$
λ_{gs}	=	1	ground stretch for soft part
λ_{gh}	=	1.428	ground stretch for hard part (cube)
λ_{gh}	=	1.274	ground stretch for hard skin (cylinder)
G_{ds}	=	1 e6 [Pa]	shear modulus soft part
G_{dh}	=	$50 \times G_{dc} = 5\,e7$ [Pa]	shear modulus stiff part (cube)
G_{dh}	=	$30 \times G_{dc} = 3\,e7$ [Pa]	shear modulus stiff part (cylinder)
χ	=	0.2	Flory parameter
Ω	=	$1.8\,e-5$ m^3/mol	water molar volume
d	=	$1\,e-6$ m^2/s	diffusivity
D_μ	=	0.41 mol/(m^2 s) · mol/J	transfer coefficient ($D_\mu = 1e9$ [mol/m^2] $\cdot D/(RT)$
τ_μ	=	$750\,e2$ s	transition time of step function
RT	=	2436 J/mol	gas constant · room temperature

$t = 200$ s. Concentration always jumps. The thickness evolution is shown with dashed black lines, and it ranges from $\simeq 2$ cm at $t = 0$ s, to $\simeq 1.1$ cm at final time; time runs from right to left. The properties of the model are listed in Table 1.

7.4 Initial, Boundary Value Problem on Free-Swollen Configuration $\mathcal{B}_o$

As done for $\mathcal{D}$, also the free swollen domain $\mathcal{B}_o$ is split into two regions; each region is the image under f_d of the corresponding regions of $\mathcal{D}$ at $t = 0$: $\mathcal{B}_{os} = f_d(\mathcal{D}_s, 0)$ is the soft region, and $\mathcal{B}_{oh} = f_d(\mathcal{D}_h, 0)$ is the hard one. It follows $\mathcal{B}_o = \mathcal{B}_{os} \cup \mathcal{B}_{oh}$; accordingly, we have the three boundaries $\mathcal{S}_{os} = f_d(\mathcal{S}_{ds}, 0)$, $\mathcal{S}_{oh} = f_d(\mathcal{S}_{dh}, 0)$ and $\mathcal{S}_{oi} = f_d(\mathcal{S}_{di}, 0)$, see Sect. 6.

Content courtesy of Springer Nature, terms of use apply. Rights reserved.

The initial, boundary value problem on $\mathcal{B}_o \times \mathcal{T}$ writes as follows. The balance of forces is:

$$\begin{aligned} 0 &= \mathtt{div}\,\mathbf{S}\,, && \text{on } \mathcal{B}_o \times \mathcal{T} && \text{bulk balance;} \\ \mathbf{S}\,\mathbf{n}_o &= \mathbf{t}\,, && \text{on } \partial_t \mathcal{B}_o \times \mathcal{T} && \text{control of traction;} \\ \mathbf{u} &= \bar{\mathbf{u}}\,, && \text{on } \partial_u \mathcal{B}_o \times \mathcal{T} && \text{control of displacement.} \end{aligned} \tag{7.138}$$

For the balance of liquid mass we shall always use a boundary condition as (5.110), where $\Delta\mu$ is the jump at the interface between two regions, or at the external boundary; the balance is split into two groups of equations. On the soft region $\mathcal{B}_{os}$ we have:

$$\begin{aligned} \dot{c}_{\mathrm{s}} &= -\mathtt{div}\,\mathbf{h} && \text{on } \mathcal{B}_{os} \times \mathcal{T} && \text{bulk balance;} \\ q &= -\frac{m_d}{|\mathbf{F}^*_{do}\,\mathbf{m}|}\,[\,\mu_d(c_s, J_{gs}, p_s) - \mu_{ext}\,] && \text{on } \mathcal{S}_{os} \times \mathcal{T} && \text{external flux;} \\ q &= -\frac{m_d}{|\mathbf{F}^*_{do}\,\mathbf{m}|}\,[\,\mu_d(c_s, J_{gs}, p_s) - \mu_d(c_h, J_{gh}, p_h)\,] && \text{on } \mathcal{S}_{oi} \times \mathcal{T} && \text{interface flux.} \end{aligned} \tag{7.139}$$

On the hard region $\mathcal{B}_{oh}$ we have:

$$\begin{aligned} \dot{c}_{\mathrm{h}} &= -\mathtt{div}\,\mathbf{h} && \text{on } \mathcal{B}_{oh} \times \mathcal{T} && \text{bulk balance;} \\ q &= -\frac{m_d}{|\mathbf{F}^*_{do}\,\mathbf{m}|}\,[\,(\mu_d(c_h, J_{gh}, p_h) - \mu_{ext}\,] && \text{on } \mathcal{S}_{oh} \times \mathcal{T} && \text{external flux;} \\ q &= -\frac{m_d}{|\mathbf{F}^*_{do}\,\mathbf{m}|}\,[\,\mu_d(c_h, J_{gh}, p_h) - (\mu_d(c_s, J_{gs}, p_s)\,] && \text{on } \mathcal{S}_{oi} \times \mathcal{T} && \text{interface flux.} \end{aligned} \tag{7.140}$$

The remark (7.126) holds also for the boundary conditions (7.139), (7.140). Finally, we have the volumetric constraint (3.29), re-written here:

$$J = \hat{J}(c) = \frac{1}{J_o} + \Omega\, c\,, \quad \text{on } \mathcal{B}_o \times \mathcal{T}\,. \tag{7.141}$$

7.5 Initial Conditions for $\mathcal{B}_{ini} = f(\mathcal{B}_o, 0)$

The initial configuration $\mathcal{B}_{ini}$ is the domain $\mathcal{B}_o$ used for the modeling: $\mathcal{B}_{ini} = \mathcal{B}_o = f(\mathcal{B}_o, 0)$, with $\mathcal{B}_o$ corresponding to μ_d. Given (6.115), the initial configuration $\mathcal{B}_{ini}$ is characterized by: the initial displacement $\mathbf{u}_o = 0$ in $\mathcal{B}_o$; the initial concentration c_{so}, pressure p_{so} and parameter J_{gs} in $\mathcal{B}_{os}$; the initial concentration c_{ho}, pressure p_{ho} and parameter J_{gh} in $\mathcal{B}_{oh}$. To set these values, we use $(5.85)_3$ for $\mathbf{S}$ and (5.95) for μ; we assume:

$$\begin{aligned} &\mathbf{F}(X, 0) = \mathbf{I}\,, && \text{trivial deformation in } \mathcal{B}_o; \\ &\mathbf{F}_g = \lambda_g\,\mathbf{I}, \quad \Rightarrow \mathbf{F}^*_g = \lambda_g^2\,\mathbf{I}, && \text{spherical distortion in } \mathcal{B}_o; \\ &\mathbf{F}_o = \mathbf{F}_{do}\,\mathbf{F}_g^{-1} = \frac{\lambda_{do}}{\lambda_g}\,\mathbf{I}, && \text{from spherical } \mathbf{F}_{do} \text{ and } \mathbf{F}_g; \\ &\mathbf{S}(X, 0) = \frac{1}{J_o}\mathbf{S}_{ge}\,\mathbf{F}_o^T - p_o\,\mathbf{F}^* = -p_{\mathrm{atm}}\,\mathbf{F}^*, && \text{stress balanced by atmospheric pressure;} \\ &\mu(c_{\mathrm{so}}, J_{\mathrm{gs}}, p_{so}) = \mu_o = 0, && \text{homogeneous chemical potential in } \mathcal{B}_{os}; \\ &\mu(c_{\mathrm{ho}}, J_{\mathrm{gh}}, p_{ho}) = \mu_o = 0, && \text{homogeneous chemical potential in } \mathcal{B}_{oh}; \end{aligned} \tag{7.142}$$

To determine the right values of J_{gs}, J_{gh}, c_{so}, c_{ho} and p_{so}, p_{ho} we follow this algorithm:

Content courtesy of Springer Nature, terms of use apply. Rights reserved.

1. We set $J_{\rm gs} = 1$, and we tune both J_{do} and $J_{\rm gh}$ to get $\mu = 0$ in both regions.
2. Given (7.142), the Neo-Hookean energy yields

$$\mathbf{S}(X,0) = \frac{1}{J_o}\mathbf{S}_{ge}\,\mathbf{F}_o^T - p_o\,\mathbf{F}^* = \left(G\,\frac{\lambda\,\lambda_g}{\lambda_{do}} - p_o\,\lambda^2\right)\mathbf{I} = -p_{\rm atm}\,\lambda^2\,\mathbf{I}\,, \quad \text{with } \lambda = 1; \tag{7.143}$$

   it follows that we can represent p_{os}, p_{oh} in terms of the parameter λ_{do} and λ_g, obtaining the same formulas as in (7.130):

$$p_{so} = G_s\,\frac{\lambda_{gs}}{\lambda_{do}} + p_{\rm atm}\,, \qquad p_{ho} = G_h\,\frac{\lambda_{gh}}{\lambda_{do}} + p_{\rm atm}\,, \tag{7.144}$$

   with G_s, G_h the shear moduli in $\mathcal{B}_{os}$ and $\mathcal{B}_{oh}$, respectively.
3. Having assumed $J_{\rm gs} = 1$, we start with the soft region. Using $(3.29)_2$ we can set the initial condition for $c_{\rm so}$:

$$c_{\rm so} = \frac{J_{do} - J_{\rm gs}}{\Omega\,J_{do}} = \frac{J_{do} - 1}{\Omega\,J_{do}}. \tag{7.145}$$

4. We use (5.95) to represent the initial chemical potential μ_o in the soft region as a function of J_{do}:

$$\begin{aligned}\mu &= \mu(c_{\rm so}, J_{\rm gs}, p_{os})\\ &= R\,T\left[\log\left(\frac{\Omega\,J_{do}\,c_{so}}{J_{gs} + \Omega\,J_{do}\,c_{so}}\right) + \frac{\chi\,J_{gs}^2}{(J_{gs} + \Omega\,J_{do}\,c_{so})^2} + \frac{J_{gs}}{J_{gs} + \Omega\,J_{do}\,c_{so}}\right] + \Omega\,p_{os}\end{aligned} \tag{7.146}$$

   Solving $\mu(J_{\rm do}) = 0$ yields $J_{\rm do}$ and $\lambda_{do} = J_{do}^{1/3}$.
5. Then, we move to the hard region to find $c_{\rm ho}$:

$$c_{\rm ho} = \frac{J_{do} - J_{gh}}{\Omega}; \tag{7.147}$$

6. We use again (5.95) to represent the initial chemical potential μ_o in the hard region as a function of $J_{\rm gh}$:

$$\mu(c_{\rm ho}, J_{\rm gh}, p_{oh}) = \mu(J_{\rm gh})\,. \tag{7.148}$$

   Solving $\mu(J_{\rm gh}) = 0$ yields $J_{\rm gh}$ and $\lambda_{gh} = J_{gh}^{1/3}$.

Eventually, we have the right values of λ_{do}, λ_{gs} and λ_{gh} that yield a uniform configuration $\mathcal{B}_{ini} = \mathcal{B}_o$ with homogeneous chemical potential $\mu = \mu_o = 0$ J/mol, and homogeneous stress $\mathbf{S}$ satisfying the boundary conditions.

7.6 Skin Effect in a Cylindrical Body

We solve the drying problem for a cylindrical specimen, using as domain $\mathcal{D}$ a cylinder with radius R_d, and same height. The cylinder has two hard domains $\mathcal{D}_h$ at the bases, and a soft domain $\mathcal{D}_s$ in between. The hard domains $\mathcal{D}_h$ are both much thinner than the cylinder height, and much stiffer with respect to the core, yielding the so called skin effect. Precisely, skin is 30 times stiffer then the core, and its thickness is $H_d = R_d/50$. At preparation state $\mathcal{B}_o$

Content courtesy of Springer Nature, terms of use apply. Rights reserved.

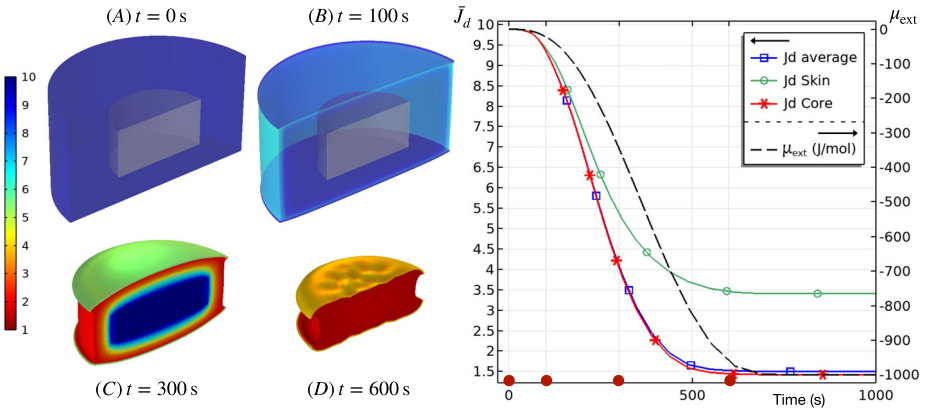

Fig. 12 Left: Four configurations $\mathcal{B}_t$ of the specimen at $t = 0$, 100, 300, 600 s; the shaded gray region in panels (A) and (B) represents the domain $\mathcal{D}$. Color legend shows swelling ratio J_d. Right: Two y-axis plot. Left y-axis: Average swelling ratio $\bar{J}_d$ versus time in the whole specimen (blue, square), in the hard skin (green, circle) and in the soft core(red, star). Right y-axis: external chemical potential μ_{ext} (black, dashed) versus time. The four red dots on the time axis correspond to the four configurations in the right)

the specimen is a cylinder in free-swelling conditions; in this example, the ground volume elements in the soft core and in hard skin are stretched by λ_{os} and λ_{oh}, respectively, with

$$\lambda_{os} = \frac{\lambda_{do}}{\lambda_{gs}} = \frac{2.146}{1} = 2.146\,, \quad \lambda_{oh} = \frac{\lambda_{do}}{\lambda_{gh}} = \frac{2.146}{1.274228} = 1.6843. \tag{7.149}$$

Thus, the stretch from dry to free swelling conditions is $\lambda_{os} = 2.146$ for the soft core, and $\lambda_{oh} = 1.6843$ for the hard skin. Geometric and materials properties of the model are listed in Table 1.

As observed in the previous example, a decreasing of the external chemical potential yields a mismatch between the hard skin and the soft core because the soft region de-swells much more than the hard one: in-plane compression builds up in the skin until wrinkling appears. Figure 12 (left) shows four configurations (only half configuration is displayed): A) Initial configuration $\mathcal{B}_o$. B) Current configuration $\mathcal{B}_t$ at $t = 100$ s; C) $\mathcal{B}_t$ at $t = 300$ s; the effect of the skin is evident, and the bases initially flat are bended outward. D) $\mathcal{B}_t$ at $t = 600$ s. The skin yields grooves on both bases, and from now on this configuration remains almost steady. Color legend shows the swelling ratio J_d; the shaded gray region in panels (A) and (B) represents the domain $\mathcal{D}$.

Figure 12 (right) is a two y-axis plot. Left y-axis: Average swelling ratio $\bar{J}_d$ versus time in the whole specimen (blue, square), in the hard skin (green, circle) and in the soft core(red, star). Right y-axis: external chemical potential μ_{ext} (black, dashed) versus time. The four red dots on the time axis correspond to the four configurations in the right.

8 Comparison Between the Two Modeling Strategies

In this section we solve the de-hydration problem for a sphere having an empty cavity, with a soft core and a hard skin, under the assumption of spherical symmetry. In particular, we solve a same problem using the two modeling approaches described insofar, that is using

Content courtesy of Springer Nature, terms of use apply. Rights reserved.

Table 2 Geometric Parameters for the 1D model

R_c	=	3 [mm]	radius cavity on $\mathcal{B}_o$ (free-swollen)
R_i	=	14.25 [mm]	radius core on $\mathcal{B}_o$ (free-swollen)
R_e	=	15 [mm]	external radius on $\mathcal{B}_o$ (free-swollen)
R_{dc}	=	$R_{oc}/\lambda_{do} = 2$ [mm]	radius cavity on $\mathcal{D}$ (domain)
R_{di}	=	$R_{oi}/\lambda_{do} = 9.5$ [mm]	radius core on $\mathcal{D}$ (domain)
R_{de}	=	$R_{oe}/\lambda_{do} = 10$ [mm]	external radius on $\mathcal{D}$ (domain)

Table 3 Materials Parameters for the 1D model

λ_{do}	=	1.5	ratio diameter($\mathcal{B}_o$)/diameter($\mathcal{D}$)
G_{dc}	=	2.12 e6 [Pa]	shear modulus core
G_{ds}	=	$50 \times G_{dc} = 1.08\,e8$ [Pa]	shear modulus skin
χ	=	0.5	Flory parameter
Ω	=	$1.8\,e-5$ m^3/mol	water molar volume
d	=	$1\,e-9$ m^2/s	diffusivity
D_μ	=	$4\,e-4$ mol/(m^2 s) $\cdot$ mol/J	transfer coefficient
p_{atm}	=	$1.01\,e5$ Pa	atmospheric pressure
τ_μ	=	$1\,e3$ s	transition time of step function
RT	=	2436 J/mol	gas constant $\cdot$ room temperature

as domain $\mathcal{D} \times \mathcal{T}$ or $\mathcal{B}_o \times \mathcal{T}$; the values of the geometric and materials parameters are in Tables 2 and 3.

The two examples are solved with the Finite Elements Method (FEM) by using the software COMSOL Multiphysics; the balance equations are written in weak form by mean of the *Weak Form* physics interface, and we implement a time evolutive problem where the only control is a time varying external chemical potential μ_{ext}, given by

$$\mu_{ext}(t) = \mu_o + (\mu_\infty - \mu_o)\, s(t/\tau_\mu)\,, \tag{8.150}$$

with $s(\cdot)$ a smooth, step-like function such that $s(0) = 0$ and $s(1) = 1$. We solve drying problems, setting $\mu_o \simeq 0$ J/mol, and $\mu_\infty \simeq -1e4$ J/mol, corresponding to a fully swollen configuration and an almost dry one, respectively.

8.1 1D Model: Bi-Domain Sphere with Spherical Symmetry

Under the assumption of spherical symmetry, we have noteworthy simplifications: both $\mathcal{D}$, $\mathcal{B}_o$ and $\mathcal{B}_\tau$ are represented by an interval, and the only non trivial component of the displacement is the radial one; relation (3.7) rewrites as

$$r = R_d + u_d(R_d, t) = R + u(R, t)\,, \tag{8.151}$$

with R_d, R, and r the radial coordinate on $\mathcal{D}$, $\mathcal{B}_o$ and $\mathcal{B}_t$, respectively; we denote with a prime the derivatives with respect to the radial coordinate, and with a superimposed dot the time derivative. In the spherical basis, the deformation tensors are represented by diagonal

Content courtesy of Springer Nature, terms of use apply. Rights reserved.

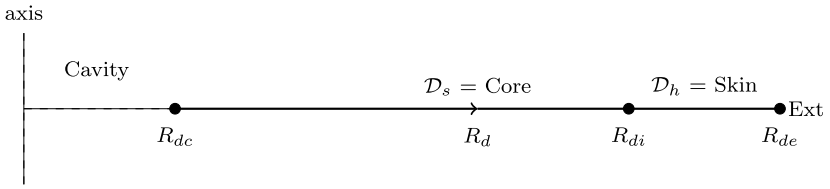

Fig. 13 The body domain $\mathcal{D}$ is made of a soft core $\mathcal{D}_s$, and hard skin $\mathcal{D}_h$, that is $\mathcal{D} = \mathcal{D}_s \cup \mathcal{D}_h$. Radial coordinate is R_d; at the interface R_{di}, the state variables concentration and pressure might jump. $\mathcal{B}_o$ and $\mathcal{B}_t$ have a same geometry: $\mathcal{B}_o = \mathcal{B}_{os} \cup \mathcal{B}_{oh}$ and $\mathcal{B}_t = \mathcal{B}_{ts} \cup \mathcal{B}_{th}$

matrices; we have:

$$\mathbf{F}_d = \begin{bmatrix} \lambda_{dr} & 0 & 0 \\ 0 & \lambda_{d\vartheta} & 0 \\ 0 & 0 & \lambda_{d\vartheta} \end{bmatrix}, \mathbf{F} = \begin{bmatrix} \lambda_r & 0 & 0 \\ 0 & \lambda_\vartheta & 0 \\ 0 & 0 & \lambda_\vartheta \end{bmatrix}, \mathbf{F}_{do} = \lambda_{do}\,\mathbf{I},\ \mathbf{F}_g = \lambda_g\,\mathbf{I},\ \mathbf{F}_o = \lambda\,\mathbf{I}, \tag{8.152}$$

where the stretches in (8.152)$_{1,2}$ are defined by:

$$\begin{aligned} &\text{On } \mathcal{D}: \quad \lambda_{dr} = 1 + u_d', \quad \text{radial stretch;} \quad \lambda_{d\vartheta} = 1 + \frac{u_d}{R_d}, \quad \text{hoop stretch;} \\ &\text{On } \mathcal{B}_o: \quad \lambda_r = 1 + u', \quad \text{radial stretch;} \quad \lambda_\vartheta = 1 + \frac{u}{R}, \quad \text{hoop stretch.} \end{aligned} \tag{8.153}$$

Note that (8.153) yields $u_d = (\lambda_{d\vartheta} - 1)\, R_d$ and $u = (\lambda_\vartheta - 1)\, R$. Also the determinants and the composition of deformations simplifies as:

$$\begin{aligned} &J_d = \lambda_{dr}\,\lambda_{d\vartheta}^2, \quad J = \lambda_r\,\lambda_\vartheta^2, \quad J_o = \lambda^3, \quad J_g = \lambda_g^3; \\ &\mathbf{F}_d = \mathbf{F}\,\mathbf{F}_o\,\mathbf{F}_g \quad \Rightarrow \quad \lambda_{dr} = \lambda_r\,\lambda_o\,\lambda_g, \quad \lambda_{d\vartheta} = \lambda_\vartheta\,\lambda_o\,\lambda_g. \end{aligned} \tag{8.154}$$

The domains $\mathcal{D}$, $\mathcal{B}_o$, and $\mathcal{B}_t$ are described as follows, see Fig. 13:

$$\begin{aligned} \mathcal{D} &= \mathcal{D}_s \cup \mathcal{D}_h = (R_{dc}, R_{di}) \cup (R_{di}, R_{de}), \\ \mathcal{B}_o &= \mathcal{B}_{os} \cup \mathcal{B}_{oh} = (R_c, R_i) \cup (R_i, R_e), \\ \mathcal{B}_t &= \mathcal{B}_{ts} \cup \mathcal{B}_{th} = (r_c, r_i) \cup (r_i, r_e), \end{aligned} \tag{8.155}$$

where R_{dc}, R_c, and r_c are the cavity radii, R_{di}, R_i, and r_i are the interface radii, and R_{de}, R_e, and r_e are the external radii. These three geometries are related by (see Fig. 14):

$$\begin{aligned} &R_c = \lambda_{do}\,R_{dc}, \quad R_i = \lambda_{do}\,R_{di}, \quad R_e = \lambda_{do}\,R_{de}; \\ &r_c = R_{dc} + u_d(R_{dc}, t) = R_c + u(R_c, t) = \lambda_{d\vartheta}(R_{dc}, t)\,R_{dc} = \lambda_\vartheta(R_c, t)\,R_c \\ &r_i = R_{di} + u_d(R_{di}, t) = R_i + u(R_i, t) = \lambda_{d\vartheta}(R_{di}, t)\,R_{di} = \lambda_\vartheta(R_i, t)\,R_i \\ &r_e = R_{de} + u_d(R_{de}, t) = R_e + u(R_e, t) = \lambda_{d\vartheta}(R_{de}, t)\,R_{de} = \lambda_\vartheta(R_e, t)\,R_e \end{aligned} \tag{8.156}$$

Content courtesy of Springer Nature, terms of use apply. Rights reserved.

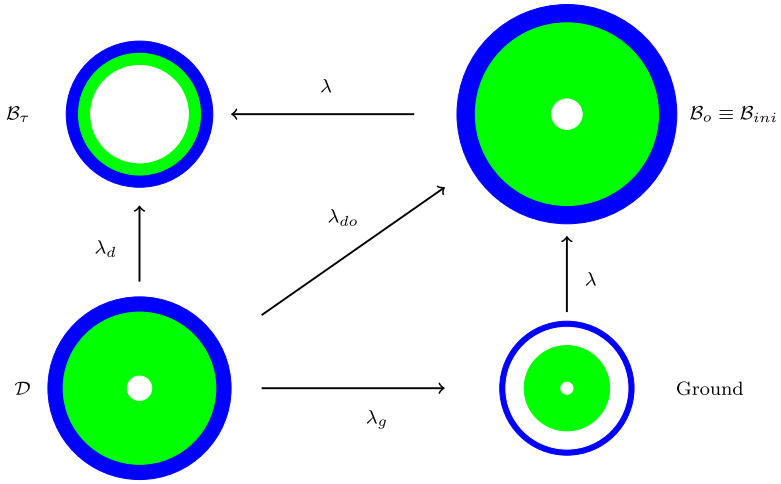

Fig. 14 The big picture: cross sections of the bi-domain sphere; soft core is green, hard skin is blue. Top: Current configuration $\mathcal{B}_t$ after drying (left); Free swollen configuration $\mathcal{B}_o$ (right). Bottom: Body domain $\mathcal{D}$ (left); Ground state of core and skin (right). Green core and blue skin are disjoint at the ground state, that is they are incompatibles at dry conditions

The ground density of elastic energy rewrites as:

$$\begin{aligned}\psi_{ge} &= \psi_{ge}(\lambda_{dr}, \lambda_{d\vartheta}, \lambda_g) = \frac{G_d}{2}\left[\left(\frac{\lambda_{dr}}{\lambda_g}\right)^2 + 2\left(\frac{\lambda_{d\vartheta}}{\lambda_g}\right)^2 - 3\right] \quad \text{on } \mathcal{D};\\ \psi_{gm} &= \psi_{ge}(\lambda_r, \lambda_\vartheta, \lambda_o) = \frac{G_d}{2}\left[(\lambda_{dr}\,\lambda_o)^2 + 2\,(\lambda_{d\vartheta}\,\lambda_o)^2 - 3\right] \quad \text{on } \mathcal{B}_o;\end{aligned} \tag{8.157}$$

8.2 The Initial, Boundary Value Problem on $\mathcal{D} = (R_{dc}, R_{de})$

We follow the same algorithm described in Sect. 7.1, and we rewrite only the equations specific of spherical symmetry. The radial and hoop reference stresses (first Piola stress), and the radial flux on $\mathcal{D}$ are given by:

$$\begin{aligned}&S_{dr} = S_{dr}(\lambda_{dr}, \lambda_{d\vartheta}, \lambda_g) = G_d\,\lambda_{dr}\,\lambda_g - p\,\lambda_{d\vartheta}^2\,, && \text{radial reference stress;}\\ &S_{d\vartheta} = S_{d\vartheta}(\lambda_{dr}, \lambda_{d\vartheta}, \lambda_g) = G_d\,\lambda_{d\vartheta}\,\lambda_g - p\,\lambda_{dr}\,\lambda_{d\vartheta}\,, && \text{hoop reference stress;}\\ &h_{dr} = -\frac{d}{RT}\,\frac{c_d}{\lambda_g^2}\,\mu_d', && \text{radial reference flux}\,.\end{aligned} \tag{8.158}$$

The corresponding current stresses on $\mathcal{B}_t$ (Cauchy) are given by:

$$\begin{aligned}&\sigma_r = \sigma_r(\lambda_{dr}, \lambda_{d\vartheta}, \lambda_g) = G_d\,\frac{\lambda_{dr}\,\lambda_g}{\lambda_{d\vartheta}^2} - p\,, && \text{radial stress;}\\ &\sigma_\vartheta = \sigma_\vartheta(\lambda_{dr}, \lambda_{d\vartheta}, \lambda_g) = G_d\,\frac{\lambda_g}{\lambda_{dr}} - p\,, && \text{hoop stress.}\end{aligned} \tag{8.159}$$

Content courtesy of Springer Nature, terms of use apply. Rights reserved.

Let us note that the radial stress in spherical coordinates is given by

$$S_{dr} = G_d\,\lambda_{dr}\,\frac{\lambda_{g\vartheta}^2}{\lambda_{gr}} - p\,\lambda_{d\vartheta}^2\,. \tag{8.160}$$

By assuming a spherical distortion $\lambda_{g\vartheta} = \lambda_{gr} = \lambda_g$, we get $(8.158)_1$. The boundary load is a pressure, both in the cavity and at the external boundary:

$$\mathbf{t}_d = -p_{in}\,\mathbf{F}_d^*\,\mathbf{m} \text{ at } r = R_{dc}, \quad \mathbf{t}_d = -p_{ext}\,\mathbf{F}_d^*\,\mathbf{m} \text{ at } r = R_{de}. \tag{8.161}$$

8.2.1 Balance Equations on $\mathcal{D} = (R_{dc}, R_{de})$

We list all the balance equation in integral form (weak form) and with the hypothesis of spherical symmetry. The balance of forces (4.51) yields the following integral contribution for the whole interval $\mathcal{D} = (R_{dc}, R_{de})$:

$$I_{df}(\tilde{u}_d, \tilde{p}, \tilde{c}_{dc}, \tilde{c}_{ds}) = \int_{R_{dc}}^{R_{de}} \Big[-S_{dr}\cdot\tilde{u}_d' - \frac{2}{R_d}\,S_{d\vartheta}\cdot\tilde{u}_d \Big] 4\pi\,R_d^2\,dR_d \tag{8.162}$$

$$+ 4\pi\,R_{dc}^2 \Big[\, p_{atm}\,\lambda_{d\vartheta}^2\cdot\tilde{u}_d \Big]_{R_{dc}} \tag{8.163}$$

$$- 4\pi\,R_{de}^2 \Big[\, p_{atm}\,\lambda_{d\vartheta}^2\cdot\tilde{u}_d \Big]_{R_{de}}\,. \tag{8.164}$$

The balance of liquid content (4.40) splits into two integral contributions, coupled through a condition at the interface R_{di}. For the core the skin we have, respectively:

$$I_{dcc}(\tilde{u}_d, \tilde{p}, \tilde{c}_{dc}, \tilde{c}_{ds}) = \int_{R_{dc}}^{R_{di}} \Big[-\dot{c}_{dc}\cdot\tilde{c}_{dc} + h_{dr}\cdot\tilde{c}_{dc}' \Big] 4\pi\,R_d^2\,dR_d \tag{8.165}$$

$$+ 4\pi\,R_{di}^2 \Big[\, m_d\,(\mu_{ds} - \mu_{dc})/h_d\cdot\tilde{c}_{dc} \Big]_{R_{di}}\,;$$

$$I_{dcs}(\tilde{u}_d, \tilde{p}, \tilde{c}_{dc}, \tilde{c}_{ds}) = \int_{R_{di}}^{R_{de}} \Big[-\dot{c}_{ds}\cdot\tilde{c}_{ds} + h_{dr}\cdot\tilde{c}_{ds}' \Big] 4\pi\,R_d^2\,dR_d \tag{8.166}$$

$$- 4\pi\,R_{di}^2 \Big[\, m_d\,(\mu_{ds} - \mu_{dc})/h_d\cdot\tilde{c}_{ds} \Big]_{R_{di}}$$

$$- 4\pi\,R_{de}^2 \Big[\, m_d\,(\mu_{ds} - \mu_{ext})/h_d\cdot\tilde{c}_{ds} \Big]_{R_{de}}\,.$$

The final integral contribution enforces the volumetric constraint; we have one equation on the whole domain $\mathcal{D}$:

$$I_{dv}(\tilde{u}_d, \tilde{p}, \tilde{c}_{dc}, \tilde{c}_{ds}) = \int_{R_{dc}}^{R_{de}} \big[(J_d - (J_g + \Omega\,c_d)\cdot\tilde{p}\,\big] 4\pi\,R_d^2\,dR_d\,. \tag{8.167}$$

The weak balance equation writes as

$$I_{df} + I_{dcc} + I_{dcs} + I_{dv} = 0\,, \quad \forall\,\tilde{u}_d, \tilde{p}, \tilde{c}_{dc}, \tilde{c}_{ds}\,, \tag{8.168}$$

with the test function $\tilde{u}_d$ compatible with the kinematics boundary conditions. The initial conditions are found using the same algorithm described in Sect. 7.2. We note that in $(8.165)_1$ there is not a source contribution at $R_d = R_{dc}$, that is the internal cavity is not permeable to solvent.

Content courtesy of Springer Nature, terms of use apply. Rights reserved.

8.3 The Initial, Boundary Value Problem on $\mathcal{B}_o = (R_{oc}, R_{oe})$

We follow the same algorithm described in Sect. 7.4, and we rewrite only the equations specific of spherical symmetry. The radial and hoop reference stresses (first Piola stress), and the radial flux on $\mathcal{B}_o$ are given by

$$\begin{aligned} S_{or} &= S_{or}(\lambda_r, \lambda_\vartheta, \lambda_o) = G_d \frac{\lambda_r}{\lambda_o} - p\,\lambda_\vartheta^2\,, && \text{radial reference stress;} \\ S_{o\vartheta} &= S_{o\vartheta}(\lambda_r, \lambda_\vartheta, \lambda_o) = G_d \frac{\lambda_\vartheta}{\lambda_o} - p\,\lambda_r\,\lambda_\vartheta\,, && \text{hoop reference stress;} \\ h_{or} &= -\frac{1}{\lambda_{do}^2}\frac{d}{RT}\frac{J_{do}\,c}{\lambda_g^2}\,\mu_d', && \text{radial reference flux}\,. \end{aligned} \tag{8.169}$$

The corresponding current stresses on $\mathcal{B}_t$ (Cauchy) are given by:

$$\begin{aligned} \sigma_r &= \sigma_r(\lambda_r, \lambda_\vartheta, \lambda_o) = G_d \frac{\lambda_r}{\lambda_o\,\lambda_\vartheta^2} - p\,, && \text{radial stress;} \\ \sigma_\vartheta &= \sigma_\vartheta(\lambda_r, \lambda_\vartheta, \lambda_o) = G_d \frac{1}{\lambda_o\,\lambda_r} - p\,, && \text{hoop stress.} \end{aligned} \tag{8.170}$$

8.3.1 Balance Equations on $\mathcal{B}_o = (R_c, R_e)$

We list all the balance equation in integral form (weak form) and with the hypothesis of spherical symmetry. The balance of forces (4.54) yields the following integral contribution for the whole interval $\mathcal{B}_o = (R_c, R_e)$:

$$I_f(\tilde{u}, \tilde{p}, \tilde{c}_c, \tilde{c}_s) = \int_{R_c}^{R_e} \Big[- S_r \cdot \tilde{u}' - \frac{2}{R} S_\vartheta \cdot \tilde{u} \Big] 4\pi\, R^2\, dR \tag{8.171}$$

$$+ 4\pi\, R_c^2 \Big[\, p_{atm}\, \lambda_\vartheta^2 \cdot \tilde{u}_d \,\Big]_{R_c} \tag{8.172}$$

$$- 4\pi\, R_e^2 \Big[\, p_{atm}\, \lambda_\vartheta^2 \cdot \tilde{u}_d \,\Big]_{R_e}\,. \tag{8.173}$$

The balance of liquid content (4.43) splits into two integral contributions, coupled through a condition at the interface R_i. For the core the skin we have, respectively:

$$I_{cc}(\tilde{u}_d, \tilde{p}, \tilde{c}_c, \tilde{c}_s) = \int_{R_c}^{R_i} \Big[- \dot{c}_c \cdot \tilde{c}_c + h_{dr} \cdot \tilde{c}_c' \Big] 4\pi\, R^2\, dR \tag{8.174}$$

$$+ \frac{4\pi\, R_i^2}{\lambda_{do}^2} \Big[m_d\, (\mu_s - \mu_c)/h_d \cdot \tilde{c}_c \Big]_{R_i}\,, \tag{8.175}$$

and

$$I_{cs}(\tilde{u}, \tilde{p}, \tilde{c}_c, \tilde{c}_s) = \int_{R_i}^{R_e} \Big[- \dot{c}_s \cdot \tilde{c}_s + h_r \cdot \tilde{c}_s' \Big] 4\pi\, R^2\, dR \tag{8.176}$$

$$- \frac{4\pi\, R_i^2}{\lambda_{do}^2} \Big[m_d\, (\mu_s - \mu_c)/h_d \cdot \tilde{c}_s \Big]_{R_i}$$

Content courtesy of Springer Nature, terms of use apply. Rights reserved.

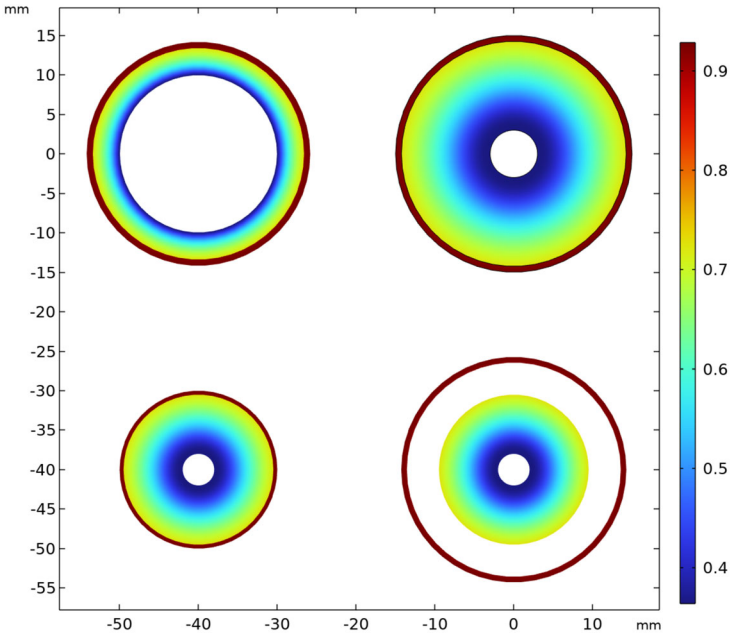

Fig. 15 Polymer fraction at $t/t_f = 1/3$ plotted on four different domains. Top left: current configuration $\mathcal{B}_t$; Top right: free-swollen configuration $\mathcal{B}_o$; Bottom left: body domain $\mathcal{D}$; Bottom right: Ground state. It is worth noting that the ground state is incompatible, that is the hard skin cannot stay attached to the soft core

$$-\frac{4\pi R_e^2}{\lambda_{do}^2}\left[m_d\left(\mu_s-\mu_{ext}\right)/h_d\cdot\tilde{c}_s\right]_{R_e}.$$

The final integral contribution enforces the volumetric constraint; we have one equation on the whole domain $\mathcal{B}_o$:

$$I_v(\tilde{u},\tilde{p},\tilde{c}_c,\tilde{c}_s)=\int_{R_c}^{R_e}\left[\left(J-(\frac{1}{J_o}+\Omega c)\right)\cdot\tilde{p}\right]4\pi R^2\,dR\,. \tag{8.177}$$

The weak balance equation writes as

$$I_f+I_{cc}+I_{cs}+I_v=0\,,\quad \forall\,\tilde{u},\tilde{p},\tilde{c}_c,\tilde{c}_s\,, \tag{8.178}$$

with the test function $\tilde{u}$ compatible with the kinematics boundary conditions. The initial conditions are found using the same algorithm described in Sect. 7.2.

The key results are summarized in Figures 15, 16, 17, and 18.

9 Conclusions

We presented a robust theoretical framework for understanding and predicting the behavior of multi-domain biological materials undergoing drying/swelling phenomena. Many of the notions used in the paper can be found scattered in many different papers, and in disparate contexts. In particular, what is specifically new is the idea of applying the notion of

Content courtesy of Springer Nature, terms of use apply. Rights reserved.

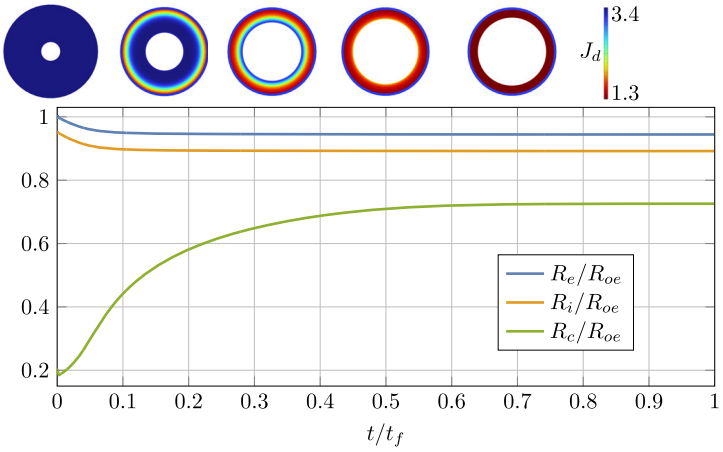

Fig. 16 Top: Five configurations $\mathcal{B}_t$ at different times; colormap shows the swelling ratio J_d. Bottom: Time evolution of the ratios r_e/R_{oe}, r_i/R_{oi}, and r_c/R_{oc}. Upon drying, the internal cavity growths much larger than the initial configuration

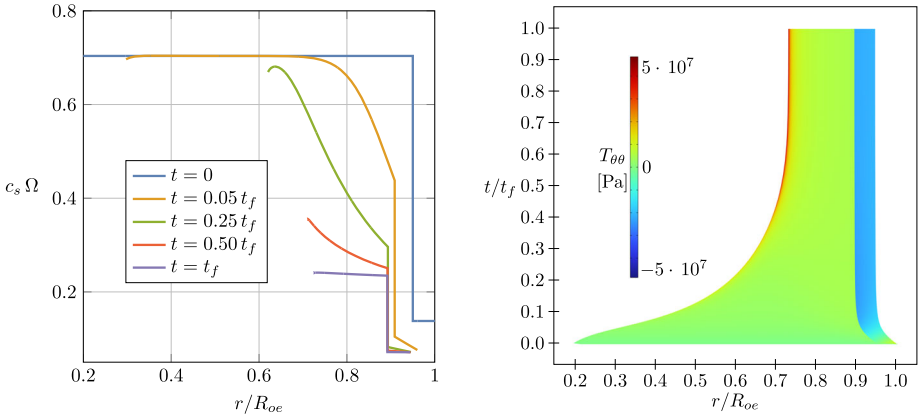

Fig. 17 Left: Current concentration c_s versus the non dimensional current radius r/R_e, at five times; the concentration always jumps at the interface. Right: current hoop stress σ_ϑ in the plane $(r/R_e, t/t_f)$; colormap shows the intensity of the stress. We note that $\sigma_\vartheta <$ (compression) in the skin and $\sigma_\vartheta > 0$ (tension) in the core

multiplicative decomposition of the strain, originally developed for plasticity, to model the swelling properties of a body made of two or more materials.

The theory has been fully developed and successfully tested on two prototypical phenomena observed in edible matter, in particular in fruits and vegetables having a soft core and a stiff skin.

Our model shows that instabilities and wrinkles formation depends on many factors; among them, global geometry (cubic, spherical, cylindrical), domains geometry (core/skin, top/bottom), many non-dimensional ratios as the thickness ratio, the stiffness ratio, and the swelling ratio. Also dynamics is fundamental, as de-hydration or swelling might happen very slowly or very fast with respect to the characteristic time of the specimen considered.

Content courtesy of Springer Nature, terms of use apply. Rights reserved.

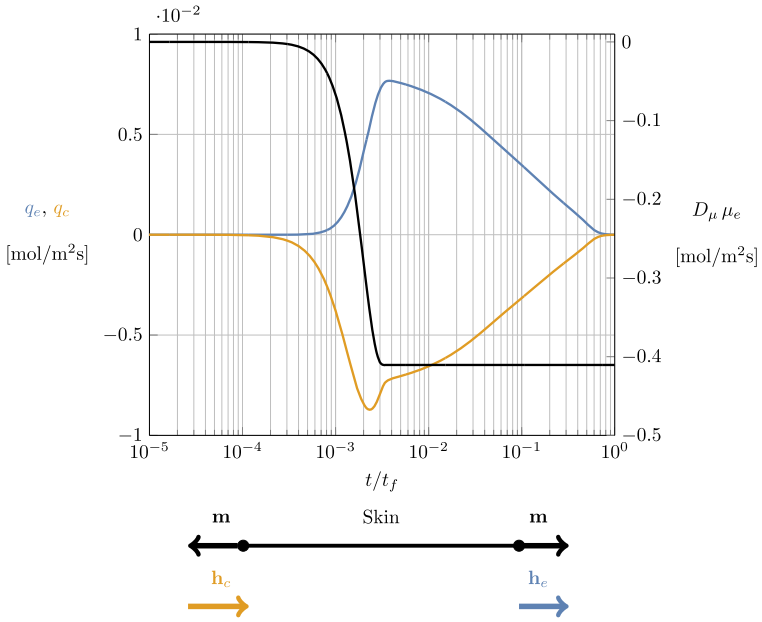

Fig. 18 Time evolution of the liquid sources at the cavity q_c and at the external boundary $q_e =$ (left y axis) and of external chemical potential (right y axis)

This framework yields many clues to tackle the problem of the selection of the body domain to describe swelling problems for other kinds of biological matter with non-homogeneous mechanical and/or chemical properties, and shows that many different modeling choices are possible, all yielding the same results.

As future directions, we envisage the possibility to apply this theory to the study of instabilities and wrinkles formation during the dehydration of soft food material having a stiff and thin skin, or having stiff inclusions inside soft bulk regions. Another interesting application is the study of tessellated food materials, where domains with different properties make a geometric pattern.

Author contributions All authors contributed equally

Funding Open access funding provided by Universitá degli Studi Roma Tre within the CRUI-CARE Agreement. This work has been supported by PNRR-M4C2-I1.1-PRIN 2022-PE1-Innovative mathematical models for soft matter and hierarchical materials-F53D2300283 0006-Funded by E.U.-NextGenerationEU. L.T. also thanks INDAM-GNFM for support.

Data Availability No datasets were generated or analysed during the current study.

Declarations

Competing interests The authors declare no competing interests.

Open Access This article is licensed under a Creative Commons Attribution 4.0 International License, which permits use, sharing, adaptation, distribution and reproduction in any medium or format, as long as you give appropriate credit to the original author(s) and the source, provide a link to the Creative Commons licence, and indicate if changes were made. The images or other third party material in this article are included in the

Content courtesy of Springer Nature, terms of use apply. Rights reserved.

article's Creative Commons licence, unless indicated otherwise in a credit line to the material. If material is not included in the article's Creative Commons licence and your intended use is not permitted by statutory regulation or exceeds the permitted use, you will need to obtain permission directly from the copyright holder. To view a copy of this licence, visit http://creativecommons.org/licenses/by/4.0/.

References

1. Amar, M.B., Ciarletta, P.: Swelling instability of surface-attached gels as a model of soft tissue growth under geometric constraints. J. Mech. Phys. Solids **58**(7), 935–954 (2010)
2. Amar, M.B., Goriely, A.: Growth and instability in elastic tissues. J. Mech. Phys. Solids **53**(10), 2284–2319 (2005)
3. Aregawi, W.A., Defraeye, T., Verboven, P., Herremans, E., De Roeck, G., Nicolai, B.: Modeling of coupled water transport and large deformation during dehydration of apple tissue. Food Bioprocess Technol. **6**, 1963–1978 (2013)
4. Bernheim-Groswasser, A., Livne, G., Nardinocchi, P., Recrosi, F., Teresi, L.: Interplay between activity, elasticity, and liquid transport in self-contractile biopolymer gels. Phys. Rev. E **109**, 014601 (2024). https://doi.org/10.1103/PhysRevE.109.014601
5. Bouman, J., Venema, P., de Vries, R.J., van der Linden, E., Schutyser, M.A.: Hole and vacuole formation during drying of sessile whey protein droplets. Food Res. Int. **84**, 128–135 (2016)
6. Cervantes, I.C., Curatolo, M., Nardinocchi, P., Teresi, L.: Morphing of soft structures driven by active swelling: a numerical study. Int. J. Non-Linear Mech. **141**, 103951 (2022). https://doi.org/10.1016/j.ijnonlinmec.2022.103951. https://www.sciencedirect.com/science/article/pii/S0020746222000282
7. Chan, A.W., Neufeld, R.J.: Modeling the controllable ph-responsive swelling and pore size of networked alginate based biomaterials. Biomaterials **30**(30), 6119–6129 (2009)
8. Chapwanya, M., Misra, N.: A soft condensed matter approach towards mathematical modelling of mass transport and swelling in food grains. J. Food Eng. **145**, 37–44 (2015)
9. Chester, S.A., Anand, L.: A thermo-mechanically coupled theory for fluid permeation in elastomeric materials: application to thermally responsive gels. J. Mech. Phys. Solids **59**(10), 1978–2006 (2011). https://doi.org/10.1016/j.jmps.2011.07.005. http://www.sciencedirect.com/science/article/pii/S0022509611001426
10. Cornwell, D.J., Okesola, B.O., Smith, D.K.: Multidomain hybrid hydrogels: spatially resolved photopatterned synthetic nanomaterials combining polymer and low-molecular-weight gelators. Angew. Chem., Int. Ed. Engl. **53**(46), 12461–12465 (2014). https://doi.org/10.1002/anie.201405098
11. Curatolo, M.: Effective negative swelling of hydrogel-solid composites. Extreme Mechanics Letters **25**, 46–52 (2018)
12. Curatolo, M., Gabriele, S., Teresi, L.: Swelling and growth: a constitutive framework for active solids. Meccanica **52**, 3443–3456 (2017)
13. Curatolo, M., Nardinocchi, P., Puntel, E., Teresi, L.: Transient instabilities in the swelling dynamics of a hydrogel sphere. J. Appl. Phys. **122**(14) (2017)
14. Curatolo, M., Nardinocchi, P., Teresi, L.: Driving water cavitation in a hydrogel cavity. Soft Matter **14**(12), 2310–2321 (2018)
15. Dai, H.H., Liu, Y.: Critical thickness ratio for buckled and wrinkled fruits and vegetables. Europhys. Lett. **108**(4), 44003 (2014)
16. De Gennes, P.G.: Scaling Concepts in Polymer Physics. Cornell University Press, Ithaca (1979)
17. Doi, M.: Soft Matter Physics. OUP, Oxford (2013). https://books.google.it/books?id=ccUaBj73PZsC
18. Dortdivanlioglu, B., Yilmaz, N.E.D., Goh, K., Zheng, X., Linder, C.: Swelling-induced interface crease instabilities at hydrogel bilayers. J. Elast. 1–17 (2021)
19. Eijkelboom, N.M., van Boven, A.P., Siemons, I., Wilms, P.F., Boom, R.M., Kohlus, R., Schutyser, M.A.: Particle structure development during spray drying from a single droplet to pilot-scale perspective. J. Food Eng. **337**, 111222 (2023)
20. Evans, A.A., Cheung, E., Nyberg, K.D., Rowat, A.C.: Wrinkling of milk skin is mediated by evaporation. Soft Matter **13**(5), 1056–1062 (2017)
21. Everaers, R.: Elasticity of c*-gels. J. Phys. II **5**(10), 1491–1500 (1995)
22. Farsheed, A.C., Thomas, A.J., Pogostin, B.H., Hartgerink, J.D.: 3d printing of self-assembling nanofibrous multidomain peptide hydrogels. Adv. Mater. **35**(11), 2210378 (2023). https://doi.org/10.1002/adma.202210378
23. Flory, P.J., Rehner, J. Jr: Statistical mechanics of cross-linked polymer networks ii. Swelling. J. Chem. Phys. **11**(11), 521–526 (1943)

Content courtesy of Springer Nature, terms of use apply. Rights reserved.

24. Forterre, Y.: Slow, fast and furious: understanding the physics of plant movements. J. Exp. Bot. **64**(15), 4745–4760 (2013)
25. Gibson, L., Ashby, M.: Cellular Solids: Structure and Properties, 2nd edn. Cambridge University Press, Cambridge (1997)
26. Giorgiutti-Dauphiné, F., Pauchard, L.: Drying drops: drying drops containing solutes: from hydrodynamical to mechanical instabilities. Eur. Phys. J. E **41**, 1–15 (2018)
27. Gulati, T., Datta, A.K.: Mechanistic understanding of case-hardening and texture development during drying of food materials. J. Food Eng. **166**, 119–138 (2015)
28. Hassan, H.M., Mumford, C.J.: Mechanisms of drylng of skin-forming materials; the significance of skin formation and a comparison between three types of material. Dry. Technol. **14**(7–8), 1763–1777 (1996)
29. Hong, W., Zhao, X., Zhou, J., Suo, Z.: A theory of coupled diffusion and large deformation in polymeric gels. J. Mech. Phys. Solids **56**(5), 1779–1793 (2008). https://doi.org/10.1016/j.jmps.2007.11.010. https://www.sciencedirect.com/science/article/pii/S0022509607002244
30. Hong, W., Liu, Z., Suo, Z.: Inhomogeneous swelling of a gel in equilibrium with a solvent and mechanical load. Int. J. Solids Struct. **46**(17), 3282–3289 (2009). https://doi.org/10.1016/j.ijsolstr.2009.04.022. https://www.sciencedirect.com/science/article/pii/S0020768309001899
31. Ilseng, A., Prot, V., Skallerud, B.H., Stokke, B.T.: Buckling initiation in layered hydrogels during transient swelling. J. Mech. Phys. Solids **128**, 219–238 (2019)
32. Jin, X., van der Sman, R.: Interaction between large deformation and moisture transport during dehydration of vegetables. Food Struct. **32**, 100269 (2022)
33. Joardder, M.U., Karim, M.: Development of a porosity prediction model based on shrinkage velocity and glass transition temperature. Dry. Technol. **37**(15), 1988–2004 (2019)
34. Kang, J., Xu, Y., Wang, C.: Instability and stress analysis for cavitation in soft graded elastic solids. Int. J. Mech. Sci. **188**, 105934 (2020)
35. Karunasena, H., Gu, Y., Brown, R., Senadeera, W.: Numerical investigation of case hardening of plant tissue during drying and its influence on the cellular-level shrinkage. Dry. Technol. **33**(6), 713–734 (2015)
36. Khalloufi, S., Bongers, P.: Mathematical investigation of the case hardening phenomenon explained by shrinkage and collapse mechanisms occurring during drying processes. In: Computer Aided Chemical Engineering, vol. 30, pp. 1068–1072. Elsevier, Amsterdam (2012)
37. Khalloufi, S., Kharaghani, A., Almeida-Rivera, C., Nijsse, J., van Dalen, G., Tsotsas, E.: Monitoring of initial porosity and new pores formation during drying: a scientific debate and a technical challenge. Trends Food Sci. Technol. **45**(2), 179–186 (2015)
38. Khokhlov, A.: Swelling and collapse of polymer networks. Polymer **21**(4), 376–380 (1980)
39. Li, B., Cao, Y.P., Feng, X.Q., Gao, H.: Mechanics of morphological instabilities and surface wrinkling in soft materials: a review. Soft Matter **8**(21), 5728–5745 (2012)
40. Liu, Y., Yang, X., Cao, Y., Wang, Z., Chen, B., Zhang, J., Zhang, H.: Dehydration of core/shell fruits. Comput. Graph. **47**, 68–77 (2015)
41. Lopez, C.G., Richtering, W.: Does Flory–Rehner theory quantitatively describe the swelling of thermoresponsive microgels? Soft Matter **13**(44), 8271–8280 (2017)
42. Lucantonio, A., Nardinocchi, P., Teresi, L.: Transient analysis of swelling-induced large deformations in polymer gels. J. Mech. Phys. Solids **61**, 205–218 (2013). https://doi.org/10.1016/j.jmps.2012.07.010
43. Matsuo, E.S., Tanaka, T.: Patterns in shrinking gels. Nature **358**(6386), 482–485 (1992)
44. Mehta, S., Raju, G., Saxena, P.: Wrinkling as a mechanical instability in growing annular hyperelastic plates. Int. J. Mech. Sci. **229**, 107481 (2022)
45. Moya, J., Lorente-Bailo, S., Salvador, M., Ferrer-Mairal, A., Martínez, M., Calvo, B., Grasa, J.: Development and validation of a computational model for steak double-sided pan cooking. J. Food Eng. **298**, 110498 (2021)
46. Nardinocchi, P., Teresi, L., Varano, V.: The elastic metric: a review of elasticity with large distortions. Int. J. Non-Linear Mech. **56**, 34–42 (2013). https://doi.org/10.1016/j.ijnonlinmec.2013.05.002. https://www.sciencedirect.com/science/article/pii/S0020746213000954. Soft Matter: a nonlinear continuum mechanics perspective
47. Nedjar, B.: Frameworks for finite strain viscoelastic-plasticity based on multiplicative decompositions. Part I: Continuum formulations. Comput. Methods Appl. Mech. Eng. **191**(15–16), 1541–1562 (2002)
48. Nelson, H., Deyo, S., Granzier-Nakajima, S., Puente, P., Tully, K., Webb, J.: A mathematical model for meat cooking. Eur. Phys. J. Plus **135**(3), 1–19 (2020)
49. Paulin, J.A., Lopez-Aguilar, J.E., Fouconnier, B., Vargas, R.O., Lopez-Serrano, F.: Revisiting the Flory–Rehner equation: taking a closer look at the Flory–Huggins interaction parameter and its functionality with temperature and concentration with nipa as a case example. Polym. Bull. 1–24 (2021)
50. Pinsky, P.M., Cheng, X.: A constitutive model for swelling pressure and volumetric behavior of highly-hydrated connective tissue. J. Elast. **129**, 145–170 (2017)

Content courtesy of Springer Nature, terms of use apply. Rights reserved.

51. Purlis, E., Cevoli, C., Fabbri, A.: Modelling volume change and deformation in food products/processes: an overview. Foods **10**(4), 778 (2021)
52. Quan, H., Kisailus, D., Meyers, M.A.: Hydration-induced reversible deformation of biological materials. Nat. Rev. Mater. **6**(3), 264–283 (2021)
53. Quesada-Pérez, M., Maroto-Centeno, J.A., Forcada, J., Hidalgo-Alvarez, R.: Gel swelling theories: the classical formalism and recent approaches. Soft Matter **7**(22), 10536–10547 (2011)
54. Sakes, A., van der Wiel, M., Henselmans, P.W., van Leeuwen, J.L., Dodou, D., Breedveld, P.: Shooting mechanisms in nature: a systematic review. PLoS ONE **11**(7), e0158277 (2016)
55. Siemons, I., Politiek, R., Boom, R., van der Sman, R., Schutyser, M.: Dextrose equivalence of maltodextrins determines particle morphology development during single sessile droplet drying. Food Res. Int. **131**, 108988 (2020)
56. Siemons, I., Veser, J., Boom, R., Schutyser, M., van der Sman, R.: Rheological behaviour of concentrated maltodextrins describes skin formation and morphology development during droplet drying. Food Hydrocoll. **126**, 107442 (2022)
57. Thibault, B., Ratti, C., Khalloufi, S.: A mapping approach to assess the evolution of pores during dehydration. Food Res. Int. **160**, 111710 (2022)
58. Truesdell, C., Noll, W.: The Non-linear Field Theories of Mechanics, 3rd edn. Springer, Berlin (2004)
59. van der Sman, R.: Biopolymer gel swelling analysed with scaling laws and Flory–Rehner theory. Food Hydrocoll. **48**, 94–101 (2015)
60. van der Sman, R.G.: Hyperelastic models for hydration of cellular tissue. Soft Matter **11**(38), 7579–7591 (2015). https://doi.org/10.1039/c5sm01032b
61. van der Sman, R., Curatolo, M., Teresi, L.: Pore development in viscoelastic foods during drying. Soft Matter **20**, 5183–5194 (2024). https://doi.org/10.1039/D4SM00201F
62. van der Sman, R., Curatolo, M., Teresi, L.: Analytical and numerical solutions of pore formation in elastic food materials during dehydration. Current Research in Food Science **8**, 100762 (2024). https://doi.org/10.1016/j.crfs.2024.100762. https://www.sciencedirect.com/science/article/pii/S2665927124000881
63. Wang, H., Cai, S.: Cavitation in a swollen elastomer constrained by a non-swellable shell. J. Appl. Phys. **117**(15) (2015)
64. Wilson, W., Van Donkelaar, C., Huyghe, J.M.: A comparison between mechano-electrochemical and biphasic swelling theories for soft hydrated tissues. J. Biomech. Eng. **127**(1), 158–165 (2005)
65. Wu, Z., Bouklas, N., Huang, R.: Swell-induced surface instability of hydrogel layers with material properties varying in thickness direction. Int. J. Solids Struct. **50**(3–4), 578–587 (2013)
66. Yan, H., Jin, B.: Influence of environmental solution ph and microstructural parameters on mechanical behavior of amphoteric ph-sensitive hydrogels. Eur. Phys. J. E **35**, 1–11 (2012)
67. Yang, S., Khare, K., Lin, P.C.: Harnessing surface wrinkle patterns in soft matter. Adv. Funct. Mater. **20**, 2550–2564 (2010). https://doi.org/10.1002/adfm.201000034
68. Yin, J., Cao, Z., Li, C., Sheinman, I., Chen, X.: Stress-driven buckling patterns in spheroidal core/shell structures. Proc. Natl. Acad. Sci. **105**(49), 19132–19135 (2008)
69. Zhou, Z., Li, Y., Wong, W., Guo, T., Tang, S., Luo, J.: Transition of surface–interface creasing in bilayer hydrogels. Soft Matter **13**(35), 6011–6020 (2017)
70. Zhou, Z., Li, Y., Guo, T.F., Guo, X., Tang, S.: Surface instability of bilayer hydrogel subjected to both compression and solvent absorption. Polymers **10**(6), 624 (2018)
71. Zimberlin, J.A., Sanabria-DeLong, N., Tew, G.N., Crosby, A.J.: Cavitation rheology for soft materials. Soft Matter **3**(6), 763–767 (2007)

Publisher's Note Springer Nature remains neutral with regard to jurisdictional claims in published maps and institutional affiliations.

Content courtesy of Springer Nature, terms of use apply. Rights reserved.

Terms and Conditions

Springer Nature journal content, brought to you courtesy of Springer Nature Customer Service Center GmbH ("Springer Nature").

Springer Nature supports a reasonable amount of sharing of research papers by authors, subscribers and authorised users ("Users"), for small-scale personal, non-commercial use provided that all copyright, trade and service marks and other proprietary notices are maintained. By accessing, sharing, receiving or otherwise using the Springer Nature journal content you agree to these terms of use ("Terms"). For these purposes, Springer Nature considers academic use (by researchers and students) to be non-commercial.

These Terms are supplementary and will apply in addition to any applicable website terms and conditions, a relevant site licence or a personal subscription. These Terms will prevail over any conflict or ambiguity with regards to the relevant terms, a site licence or a personal subscription (to the extent of the conflict or ambiguity only). For Creative Commons-licensed articles, the terms of the Creative Commons license used will apply.

We collect and use personal data to provide access to the Springer Nature journal content. We may also use these personal data internally within ResearchGate and Springer Nature and as agreed share it, in an anonymised way, for purposes of tracking, analysis and reporting. We will not otherwise disclose your personal data outside the ResearchGate or the Springer Nature group of companies unless we have your permission as detailed in the Privacy Policy.

While Users may use the Springer Nature journal content for small scale, personal non-commercial use, it is important to note that Users may not:

1. use such content for the purpose of providing other users with access on a regular or large scale basis or as a means to circumvent access control;
2. use such content where to do so would be considered a criminal or statutory offence in any jurisdiction, or gives rise to civil liability, or is otherwise unlawful;
3. falsely or misleadingly imply or suggest endorsement, approval , sponsorship, or association unless explicitly agreed to by Springer Nature in writing;
4. use bots or other automated methods to access the content or redirect messages
5. override any security feature or exclusionary protocol; or
6. share the content in order to create substitute for Springer Nature products or services or a systematic database of Springer Nature journal content.

In line with the restriction against commercial use, Springer Nature does not permit the creation of a product or service that creates revenue, royalties, rent or income from our content or its inclusion as part of a paid for service or for other commercial gain. Springer Nature journal content cannot be used for inter-library loans and librarians may not upload Springer Nature journal content on a large scale into their, or any other, institutional repository.

These terms of use are reviewed regularly and may be amended at any time. Springer Nature is not obligated to publish any information or content on this website and may remove it or features or functionality at our sole discretion, at any time with or without notice. Springer Nature may revoke this licence to you at any time and remove access to any copies of the Springer Nature journal content which have been saved.

To the fullest extent permitted by law, Springer Nature makes no warranties, representations or guarantees to Users, either express or implied with respect to the Springer nature journal content and all parties disclaim and waive any implied warranties or warranties imposed by law, including merchantability or fitness for any particular purpose.

Please note that these rights do not automatically extend to content, data or other material published by Springer Nature that may be licensed from third parties.

If you would like to use or distribute our Springer Nature journal content to a wider audience or on a regular basis or in any other manner not expressly permitted by these Terms, please contact Springer Nature at

onlineservice@springernature.com